MODEL TESTS OF A SCALE 1 : 10 PHASE - CONTROLLED WAVE-POWER BUOY OF TYPE N2 IN THE SEA.

Authors

LARS CHR. IVERSEN

PER MAGNE LILLEBEKKEN

INSTITUTT FOR EKSPERIMENTALFYSIKK

NORGES TEKNISKE HØGSKOLE

TRONDHEIM, NORWAY

UNIVERSITETET I TRONDHEIM
NOREGS TEKNISKE HØGSKOLE
INSTITUTT FOR EKSPERIMENTALFYSIKK

Jan. 1983

MODEL TESTS OF A SCALE 1:10 PHASE-CONTROLLED WAVE-POWER BUOY OF TYPE N2 IN THE SEA

Authors: L.C. Iversen
P.M. Lillebekken

The work presented in this report has received its financial funding from Olje- og energidepartementet (The Royal Ministry of Petroleum and Energy).

ABSTRACT

This report describes model testing of a phase-controlled wave-power buoy of type N2 in Trondheimsfjorden during 1981 and 1982. The diameter of the model buoy was 1 m and thus the model scale was 1:10. During the experiments it was, however, found that the actual typical wave period at the testing site was somewhat small compared to the 1:10 scale. The latching mechanism used on the model was of a wedge-shaped self-latching type. The buoy was placed approximately 100 m from shore. The water depth was 4.6 m at low ebb. The signal cables were taken from the buoy on board a fleet approximately 4 m away from the buoy. From the fleet the cables were brought to shore under water. A computer on shore was used for wave prediction and phase control as well as for data logging and data analysis.

The wave prediction was based on the Kalman filtering technique combined with parameter estimation. This method had earlier been used with success in plane waves in a model tank. One of the main purposes with the model tests in Trondheimsfjorden was therefore to try out this method in a real sea environment. Most of the time the wave pressure measured below the buoy at the anchoring rod was used as input signal to the Kalman filter. Alternatively the pressure measured at a rigg located approximately 3 m away from the buoy was used.

Another main purpose with the model tests was to verify the theoretical estimates for the power absorption. The absorbed pneumatic power was measured by using a calibrated orifice. The friction loss was found by measuring the rod force together with the position of the buoy relative to the rod.

The model tests showed that the present wave prediction technique did not, in most situations, give a satisfactory phase-control. The reason for this was, however, only partly due to factors that

would be similar in the case of a full-scale buoy at the coast. One problem specific for the model buoy was that the wave period at the testing site most of the time was too close to the natural period of the buoy. Further, the typical wave spectrum at the testing site seemed to be broader both in frequency and direction than what should be expected at the coast. Another problem with the model buoy was that it had a smaller resistance against tilting than that for the full scale buoy.

Only for very small power levels (< 30 W) it was found that the power absorbed by the model buoy was in agreement with the theoretical estimate. For higher power levels the absorbed power was considerably smaller than the theoretical estimate. The analysis of the results shows that it is reasonable to suspect this deviation mainly to be caused by large viscous losses as the water level inside the buoy oscillates. These viscous losses can be significantly reduced by increasing both the radius of curvature and the area at the inlet to the internal chamber of the buoy.

CONTENTS

1. INTRODUCTION

The Wave Power Group at Institutt for eksperimentalfysikk, NTH, decided in February 1981 to establish a testing facility in Trondheimsfjorden. The main objectives for the work at this testing facility were intended to be:

1. Hydrodynamical testing of wave power devices in scale approximately 1:10.
2. Mechanical testing of components.
3. Trying out wave prediction and phase control in a real sea state.
4. Getting experience in performing experiments outdoor at sea.

A site was chosen approximately 15 km west of Trondheim.

In 1981 and 1982 a scale 1:10 model of the wave power buoy N2 [1] has been tested. All together the buoy has been out in sea for 114 days divided into the following five periods

A:	11. Sep. 81 - 9. Oct. 81	- 28 days
B:	8. Feb. 82 - 12. Feb. 82	- 4 days
C:	19. Apr. 82 - 18. May 82	- 30 days
D:	15. Jun. 82 - 1. Jul. 82	- 16 days
E:	19. Aug. 82 - 24. Sep. 82	- 36 days

This report presents the experimental work and results for these testings. In the report the five different testing periods will be refered to by using the letters A, B, C, D, E as given above.

2. THE FIELD STATION

2.1 Location

In order to find an appropriate site for the field station, some investigations were made in mars 1981. The main aspects were water depth, current velocity and fetch. Access to electric power, telephone and so on were also taken into consideration.

Measurements of current velocity and depth were made at three places, all lying west of Trondheim. The most favourable as regards distance to NTH had to be left out because of a very steep shore and large depth near land. As the other two places were situated rather near each other, and one of them made it possible to benefit from already existing installations, this was chosen. See fig. 1.

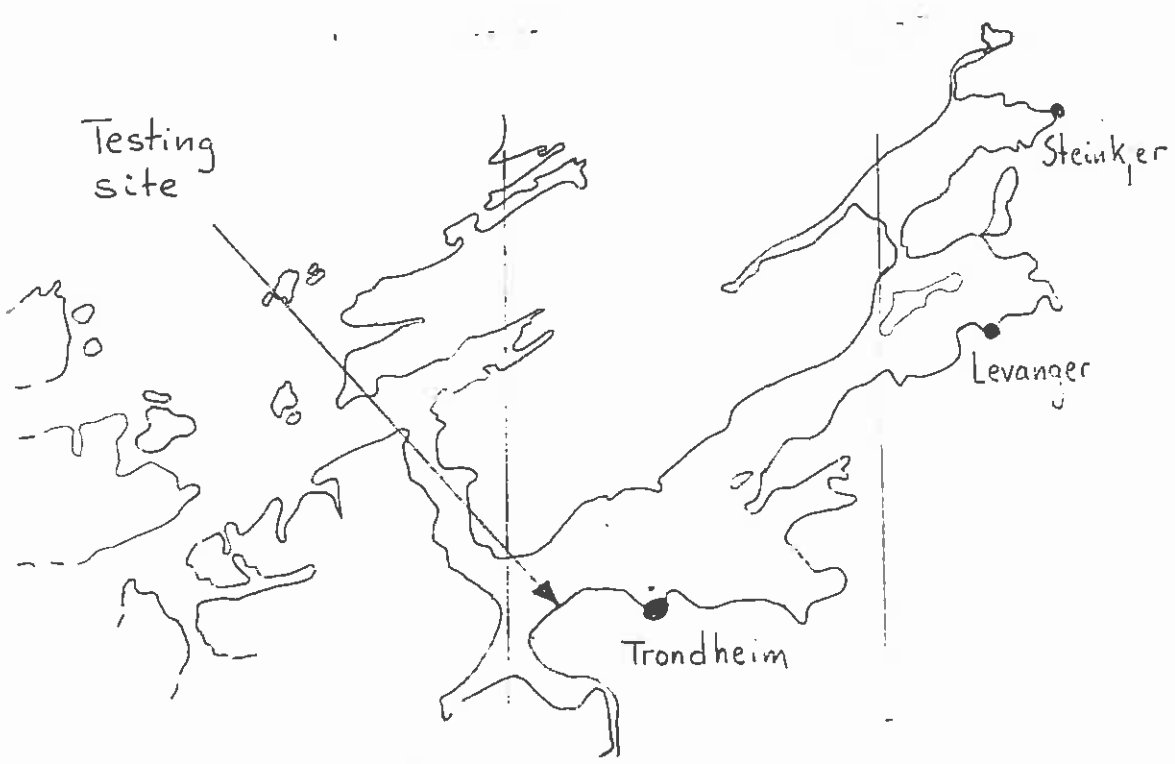

Fig. 1 The testing facilities were located by Trondheimsfjorden about 15 km from Trondheim.

2.2 Layout

The gentle slope of the sea bed had one drawback, the device, which was a buoy with a rod through it, had to be brought rather far out to reach proper depth. The requirement was a depth of 4.6 m at spring ebb, and this was obtained about 100 m from land.

Fig. 2 shows the entire arrangement. The fleet was built to be a steady working platform, and if necessary, it could be moved to the buoy.

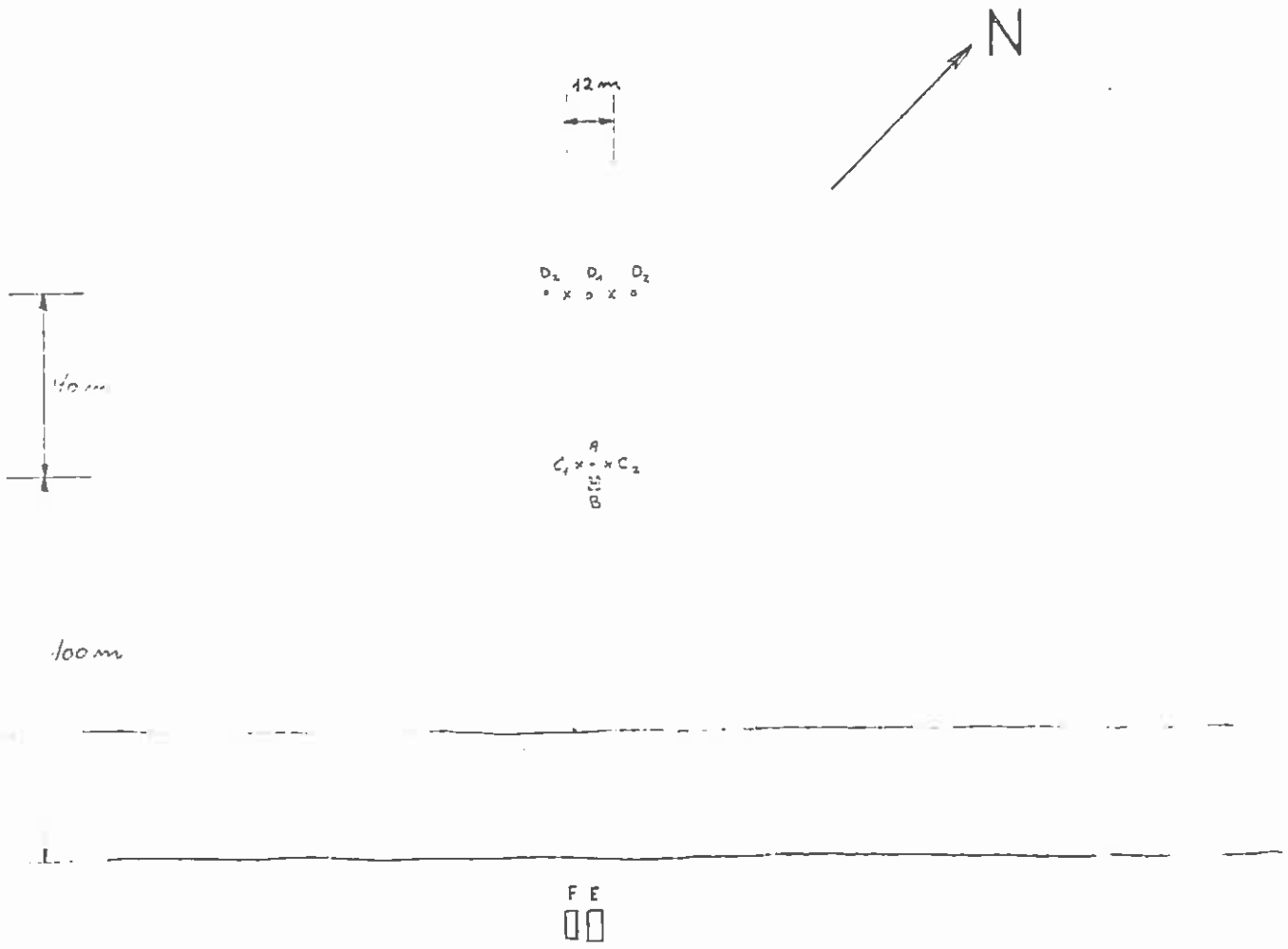

Fig. 2 The buoy A lied about 100 m from shore. B is a fleet. C_1 and C_2 are wave probes, D_1 and D_2 are floats used for mooring purposes. On land is seen the cabin, E, and the storage house, F.

2.3 Cabin

No experiments could be done without somewhere to place instruments and do work. In addition a computer was necessary to run the experiments and a cabin with two rooms was bought, the room for the computer fitted with air condition. Another house was hired for storage of chains, ropes, grapnels and so on.

2.4 The computer

The computer at the testing facility serves the following purposes:

a) Data logging.
b) Phase control.
c) Data analysis.

Both data-logging and phase control are real-time tasks. The sampling period has to be significantly smaller than the wave period. Further, the computer has to have capacity for the computational burden after each sample in connection with wave prediction and phase control. A VAX 11/750 together with LPA11-K Laboratory Peripheral Accelerator was chosen [2]. The configuration is shown in fig. 3. A software system for process controlling by such a configuration was developed [3]. All registrations were performed with sampling period $\Delta t = 0.05$ sek.

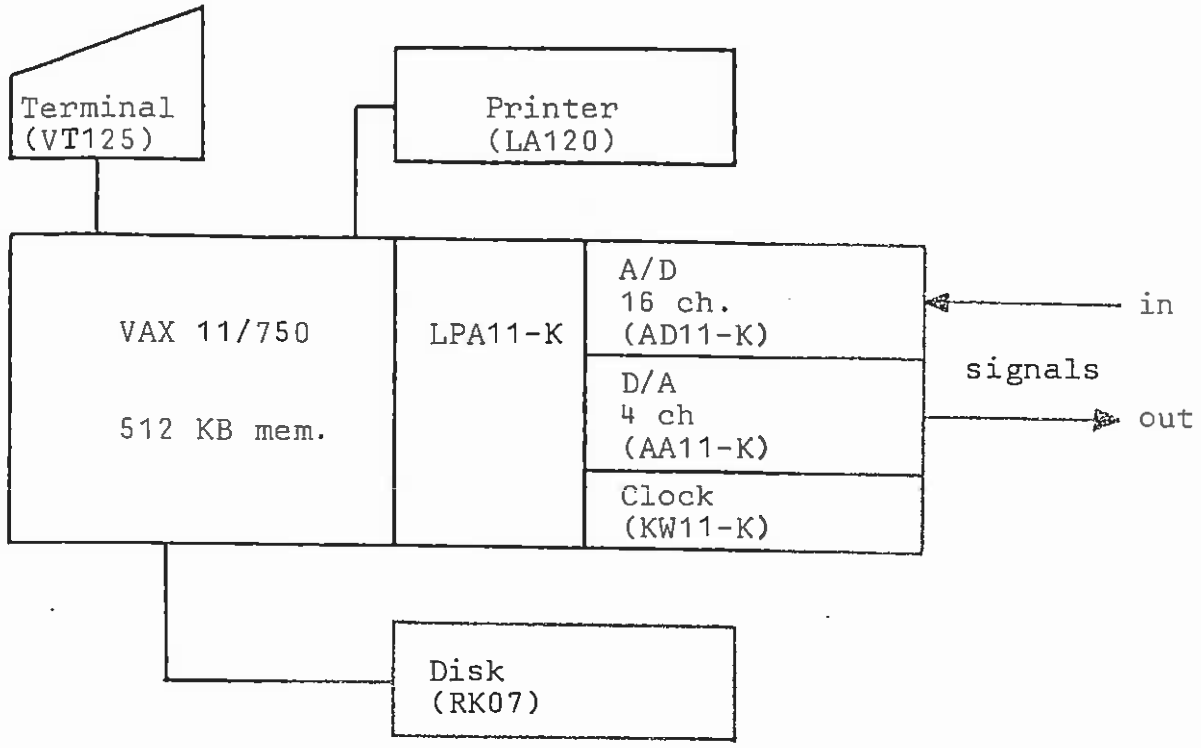

Fig. 3 The computer configuration.

2.5. Flåt

The flåt had a deck of wood with blocks of cell plastics under it.

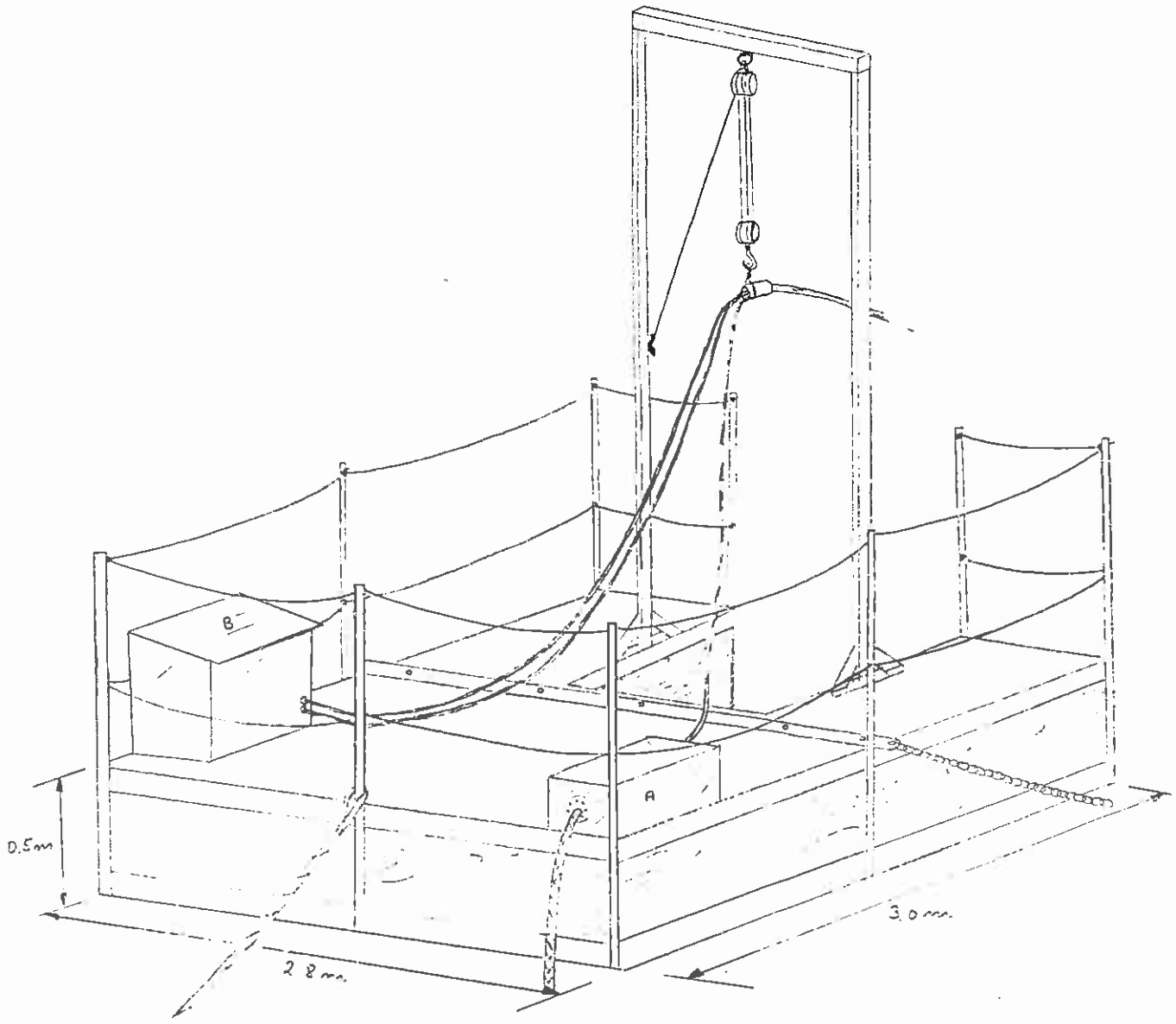

Fig. 4 The flåt was given a U-form and a rigging with block and tackle. A is a connection box and B a hydraulic aggregate. If necessary the buoy could be moved into the U and lifted. However, this operation required calm water.

The fleet was primaraly moored (fig. 5) by one rope to land and two chains to grapnels on 15 kg each, but this proved to be too weak and the grapnels were replaced by two railway wheels of 200 kg each.

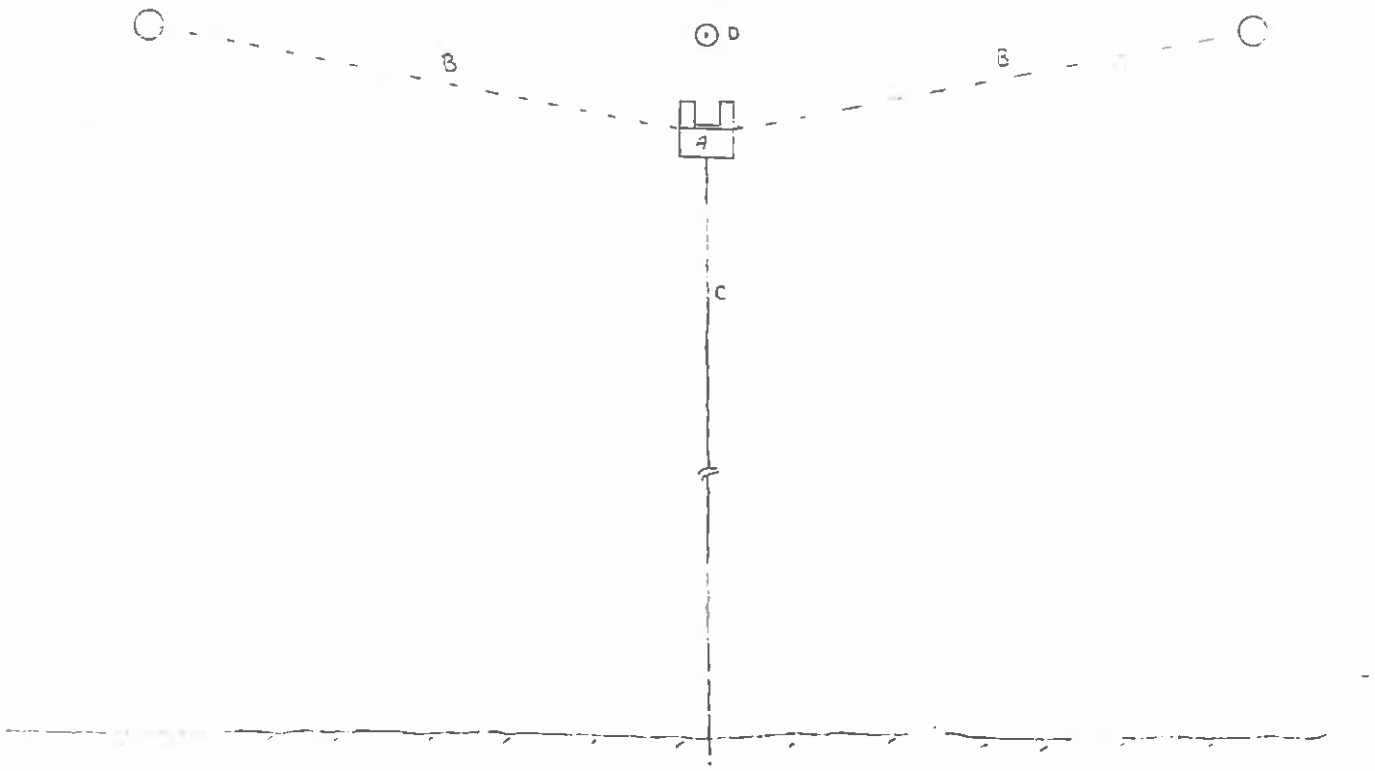

Fig. 5 The mooring of the fleet , A. B are chains (40 m) to railway wheels on the sea bed and C is a rope to shore (100 m). D is the buoy.

3. THE N2-BUOY

3.1 General view

The energy converting system is shown in fig. 6.

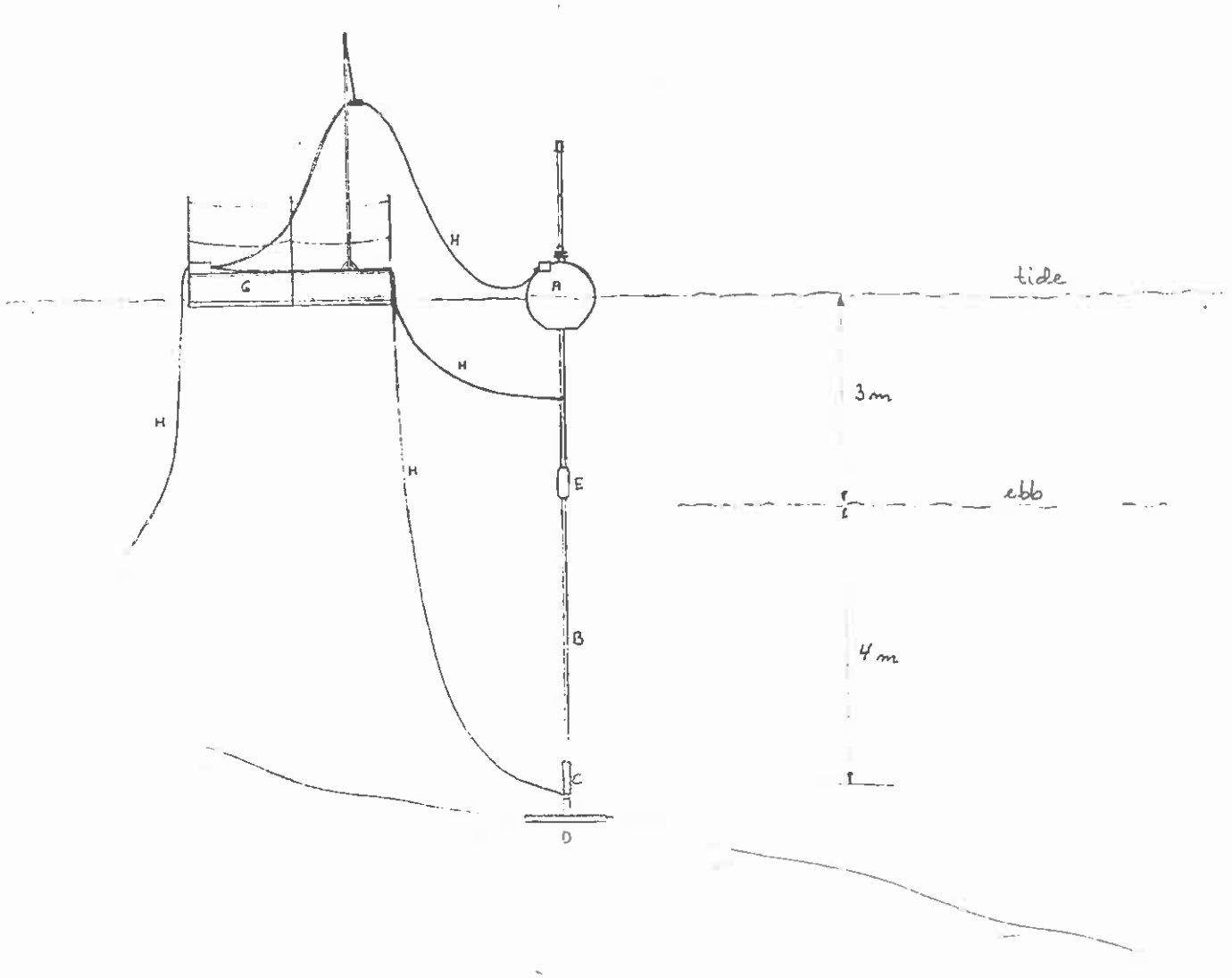

Fig. 6 The buoy, A, moves up and down along a tubular aluminium rod, B. An universal joint, C, connects the rod to a railway wheel of 500 kg on the sea bed, D. The weight, E, ensures that the rod has an equilibrium vertical position and is connected to the buoy by two wire ropes. F is a wave probe. The fleet, G, and the cables, H, are indicated.

The wave probe indicated in fig. 6 was used for the first time in period C. In period A pressure transducers were mounted in the rod itself, but they were never used because the buoy was not operative in periode A and the transducers didn't stand the tough environments and were not used later.

3.2 The buoy

The buoy hull was made of plexiglas covered with two layers of glass fiber on the outside. In order to lower viscous losses the surface was smoothed and painted.

The buoy was not quite spherical. There was an opening in the lower end. To aviod "slurping" of air round the edge, the hull was somewhat expanded downwards for a sphere. An inner sylinder provided buoyancy, and the buoy was intended to be half submerged at equilibrium. However, cabels, hoses etc. were heavier than expected, and the buoy floated about 5 cm too deep.

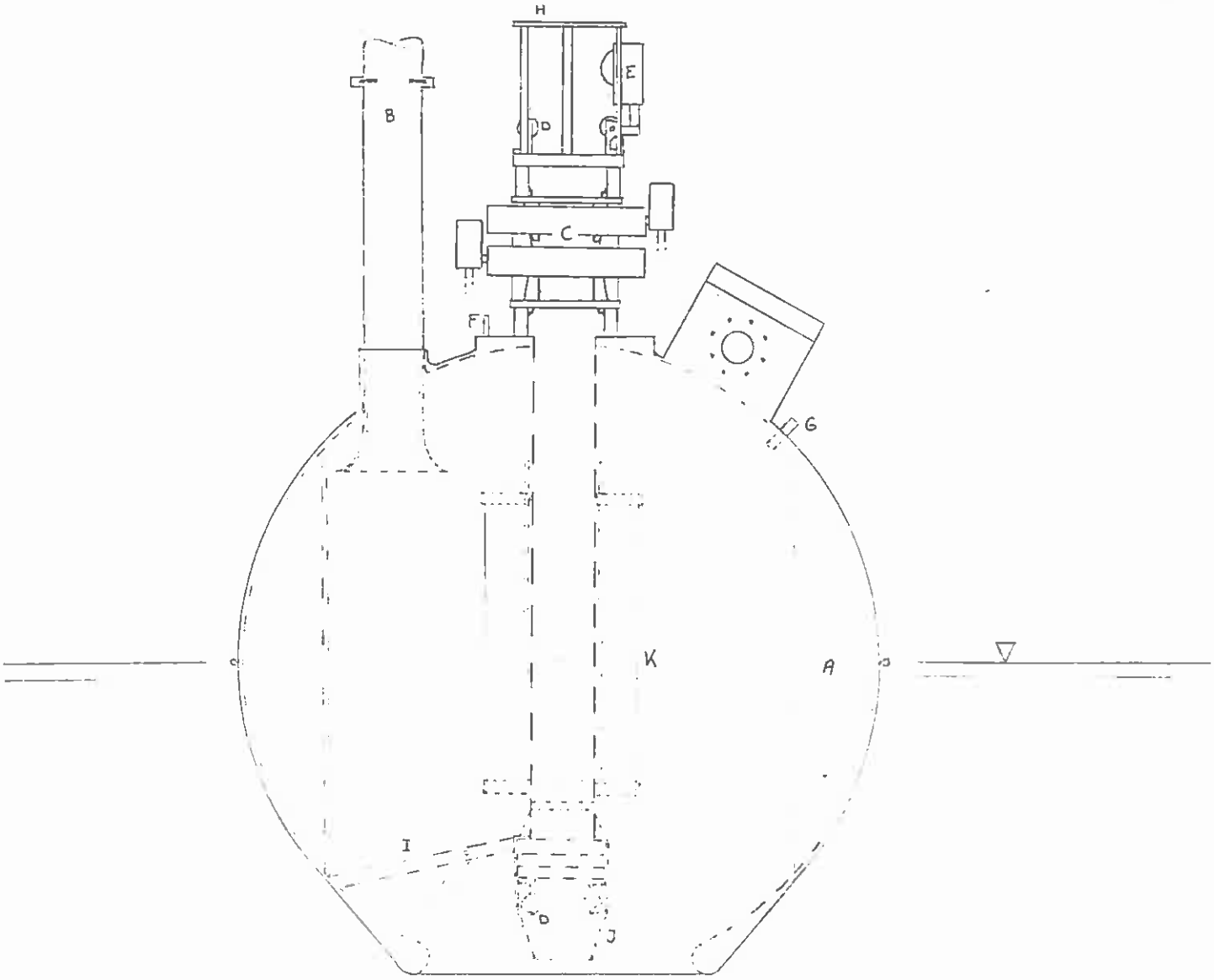

Fig. 7 The volume A provides buoyancy, B is the pneumatic power take off and C is the latching mechanism. The buoy is guided along the rod by rollers D. E, F and G illustrate the position, acceleration and chamber pressure detectors, respectively. H is a buffer and I shows one of three steel stays. The housing J was used in period E to reduce viscous losses. K is a level transducer. Electric cabels are omitted.

3.3 Power absorption

Because of the opening in the bottom, there was a water column inside the buoy. This acted as a piston and pumped air through an orifice. See fig. 7, detail B. After calibration, [4], the volume stream as function of the pressure drop over the orifice was known and the product of these two quantities was the power drained.

Another method was also tried, mostly as a chech. It was to measure the changes in water level inside the buoy and use this to calculate the volume stream. However, this was not a success. See chapter 4.4.

3.4 Guiding rollers

In order to obtain sufficient precision for the latching mechanism and in addition minimise friction forces,both the buoy and the weight were fitted with rollers. First time in sea (period A) there were ball bearings intended to be made of stainless steel. By mistake, this did not square with the facts and after one month several bearings were completely destroyed due to corrosion. This probably was the reason for an accident in october-81 when the buoy stuck to the rod on ebb and then was wholly submerged and sank when the water rised. Before period B stainless steel ball bearings were examined in the laboratory, but this steel was not found to be usable in sea environments either. In the short period B the ball bearings were temporary replaced by small rollers of PTFE, but they got too small to stand the stress and therefore a new desigh with bigger rollers were developed before period D. See fig. 8. The roller material this time was a self-lubricating type of nylon with low water absorption ($\leqslant$ 1% after 24 h).

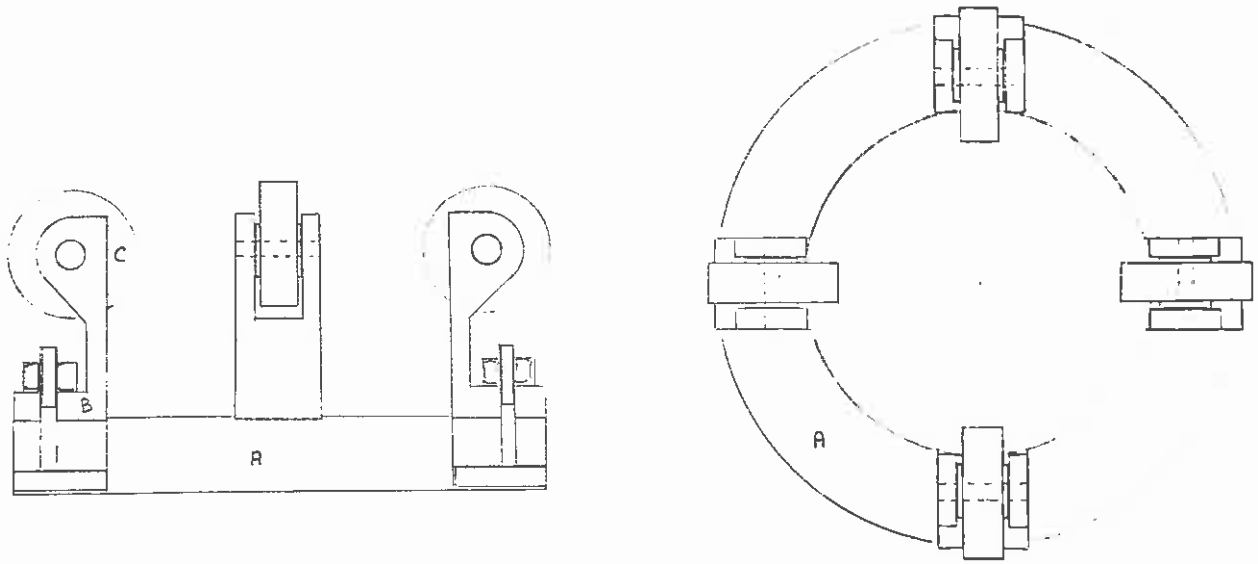

Fig. 8 Guiding rollers on the buoy. On a ring ,A, four brackets, B, with rollers ,C, are mounted. The ring is made of aluminium, the bracket and the shaft journal of stainless steel.

The roller supporting brackets on the weight were slightly different from those on the buoy because the latter were designed to take strain gauges.

3.5 The latching mechanism

The latching mechanism (see fig. 9a and b) was based on a principle of wedging.

Shortly before the buoy changes direction of movement, say in the lower position, oil is supplied through a three-way solenoid valve into channel,A, and the pistons,B, move and press the latching blocks,C, against the rod. The blocks are wedgeshaped.

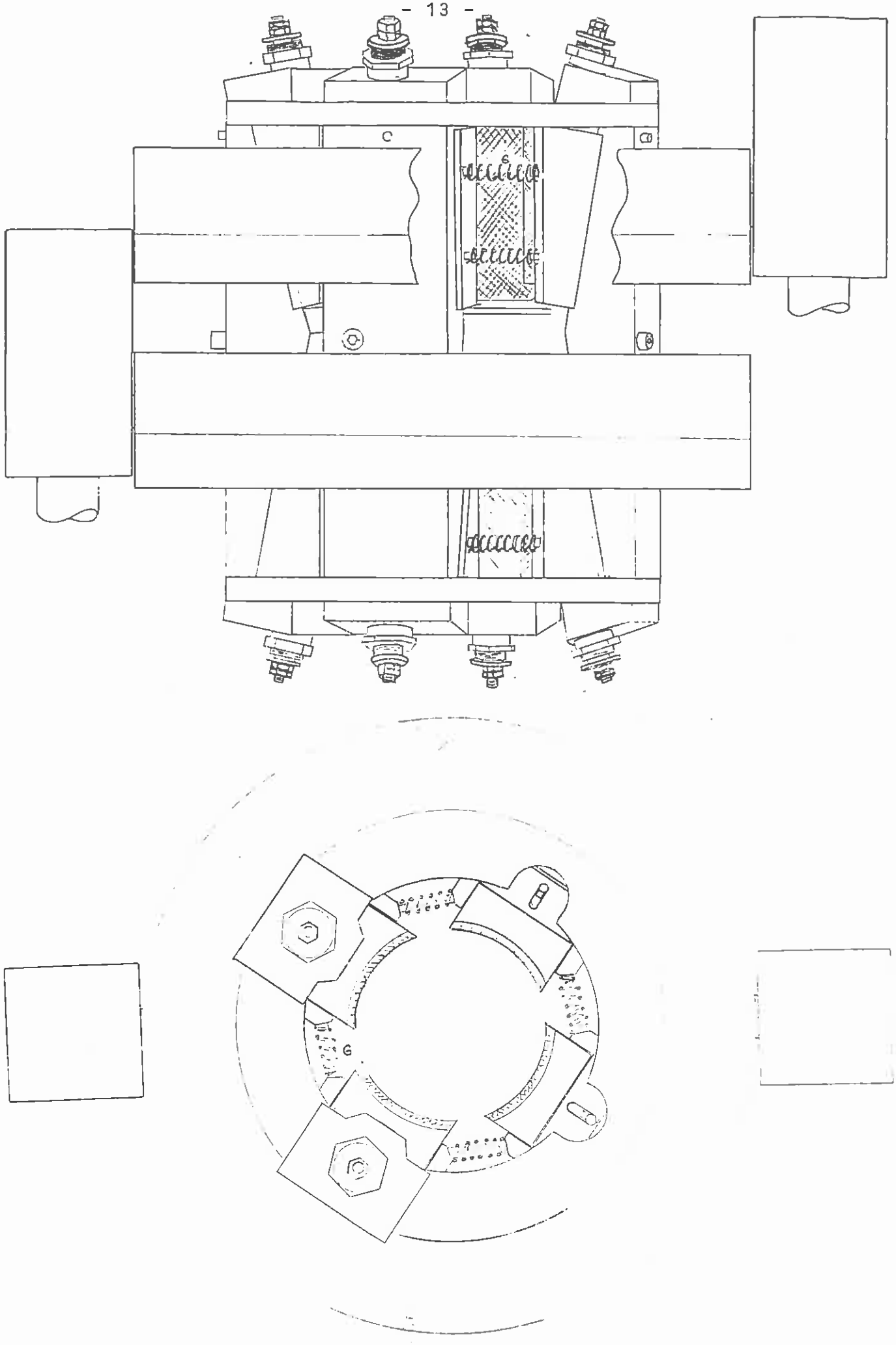

Fig. 9a The latching mechanism. The next figure shows details.

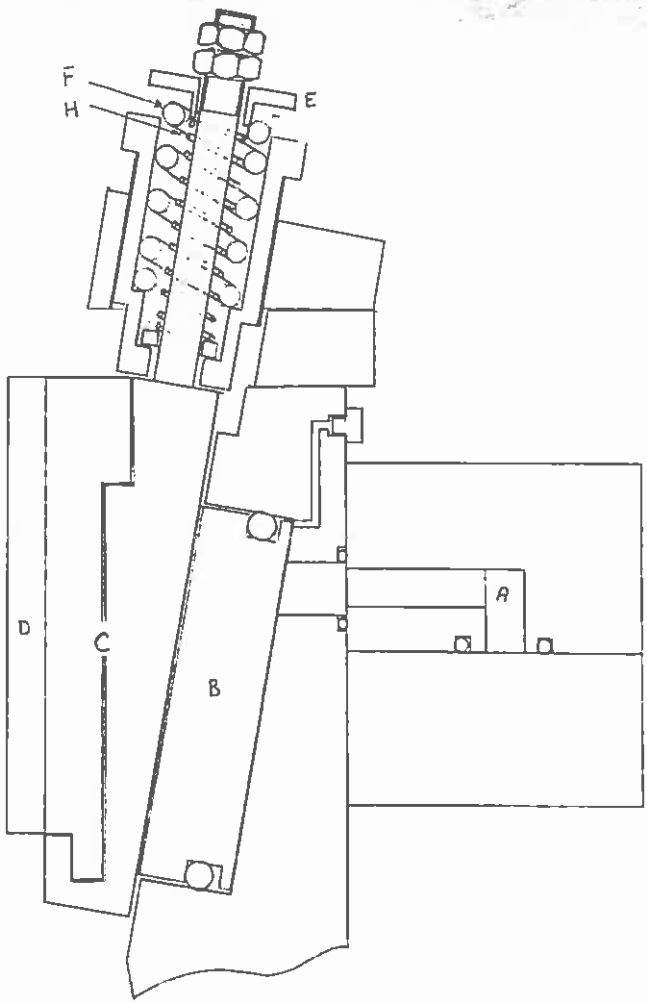

Fig. 9b Details of the latching mechanism. One of eight wedge units.

Therefore, if the friction between rod and friction lining,D, is sufficient, the buoy will jam when it begins to move upward. The oil pressure behind the pistons increases to about 10 bar because a non-return valve prevent the oil from flowing back into the pressure hose (about 3 bar). It is important that there is no air pockets in the mechanism. Otherwise, the pistons will move significantly backward as the air is compressed, and the buoy will move until sufficient normal forces against the rod is obtained. This lead to unnecessary friction losses and high stress on the whole construction because the buoy is not latched when the velocity is zero, but has to be retarded.

When it is time to release the buoy, the solenoid valve is deenergized, and exhausts the sylinder pressure. The pistons are forced backward by the blocks until the washers E get into contact with the strong springs F. Then the blocks snap back, and the springs G minimise any further contact between rod and friction lining. The springs H prevent the springs F from getting in contact with the washers at the very moment of latching.

From the beginning, the plan was to run the latching mechanism by fresh water, and a pump system on land with a pressure hose out to the fleet was almost ready. Then it was decided to run the experiments during the winter as well. Therefore oil had to be used instead. This required a return line. Thus, the pressure source was placed on the fleet in a special watertight box. The whole hydraulic system is shown in fig. 10.

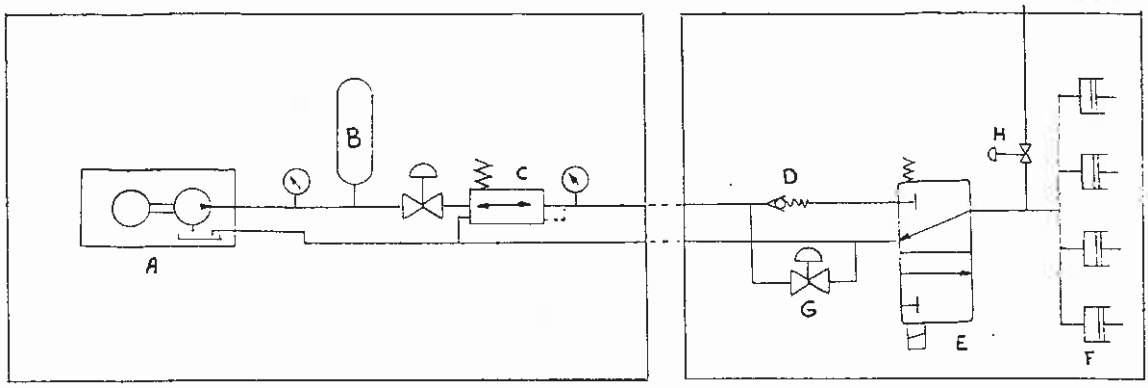

Fig. 10 The hydraulic system.
A small pump, A, charges an accumulator, B, and a pressure regulator, C, provides the pressure to the cylinders, F. D is a non-return valve and E is a 3-way solenoid valve. When the valve G is opened, a high velocity of flow is obtained and possible air in the hoses is driven out. The latching mechanism has separate air outlets, H.

The first experiences with the latching mechanism in sea was gained in period B and afterwards some details were changed. The pistons were originally made of PTFE and too accurately adapted to the cylinders. Rather big forces were sometimes necessary to press them backwards after releasing. Before period C , new pistons with less diameter were made (of POM). Tangentiell springs (fig. 9a,G) were mounted to counterbalance friction forces between o-ring and cylinder wall.

Another important matter was the centering of the rod relative to the mechanism (the guide rollers). The tolerances between rod and friction lining appeared to be too small and was increased before period C.

During the experiments the electric valves did not always work and had to be exchanged many times. There were also problems

with too less friction because of oil or fouling at the rod. Such occational problems were difficult to handle. In waves it was seldom possible to do adjustments and corrections, and in calm water the function could not be tried out.

3.6 Restoring

In waves the buoy and the rod will tend to tilt, and there was a need for righting force to prevent the buoy from moving off the rod. The weight, see fig. 6, gave a righting force proportional to its mass (35 kg) and distance to the buoy (2.8 m), but this was not enough. At first, the weight was relativly light, being determined by the buoyancy of the buoy. Secondly, tidal range could be more than 3 m, and the rod must be long enough to handle this. Therefore it would rise roughly 5 m above water level on ebb and the system could tilt to an inclined position even in calm, currentfree water. So the buoy was secured by guys to avoid collision with the fleet or the pressure-probe riggs.

To make sure that the buoy did not move off the rod at extreme flood and high waves, a stopping devise was designed (fig. 11)

The shape of the weight was the same in all periods except for E when it was modified in order to reduce viscous losses (fig. 12).

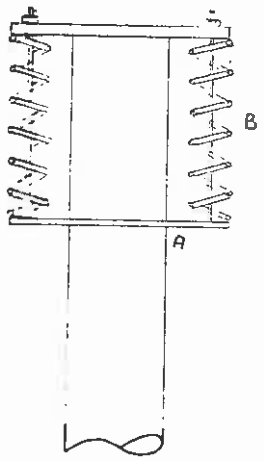

Fig. 11 The stopping device which was screwed on to the top of the rod. If the buoy reaches the plate, A, the springs, B, are pressed together and the thrust is damped. See also fig. 6 and 7.

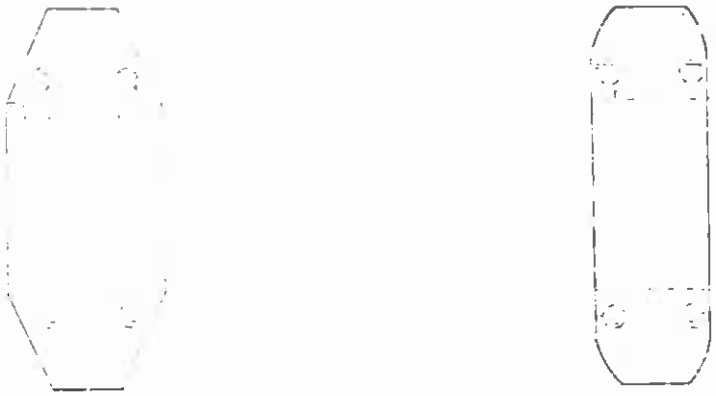

Fig. 12 The weight to the left was used in period A, B, C and D while that to the right was used in period E. The lead element (hatched) is the same in both. The guiding rollers are indicated.

3.7 Mooring

To permit angular movement, the mooring rod was connected to the anchor through an universal joint. As a stainless steel joint was hard to procure, a standard joint for tractor power take-off was used. A load cell was mounted above the joint, and all was covered with a hose filled with grease. See fig. 13. This turned out to be a good way of protection and there was never any problem with water penetration.

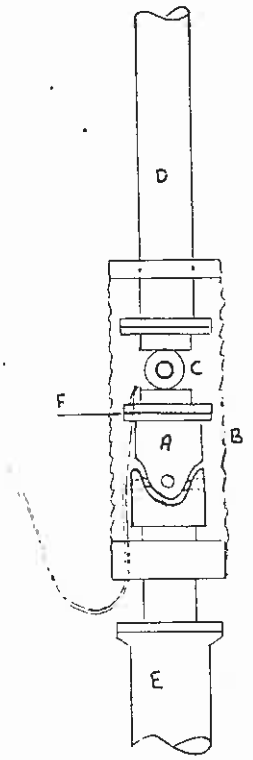

Fig. 13 The joint,A,at the bottom is protected by a hose, B , filled with grease. C is a load cell with strain gauges. D is the rod (aluminium) and E is the shaft of the railway wheel (steel). F is electric insulation.

3.8 Launching

A boat with a cargo boom was hired to bring out and position the system. The buoy and the weight were taken on board in Trondheim while the rod was stored at the field station. The railway wheel was stored at the sea bed and only raised for coupling/uncoupling of the rod.

4. INSTRUMENTATION

4.1 Wave probes

All the wave measurements were based on pressure transducers. In period A they were mounted inside the rod itself (see fig. 14), but they did not stand up to that tough environments for any length of time and after one month they were all destroyed. These transducers were connected to bridge amplifiers on shore.

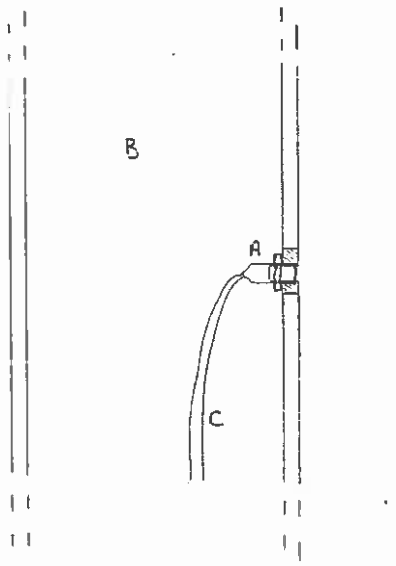

Fig. 14 From the beginning pressure transducers, A, were mounted inside the rod,B. The cables, C, where taken to shore through a separate hose.

Later another type was used where both transducer and amplifier was integrated on a small chip. To protect against sea water they were placed in an aluminium housing with openings covered with a rubber diaphragm.

The housings were then filled with silicon oil. When all air was let out, the diaphragm moved very little and its stiffness was ignored. There were three different designs.

A. The collar on the mooring rod (fig. 5 and 14)

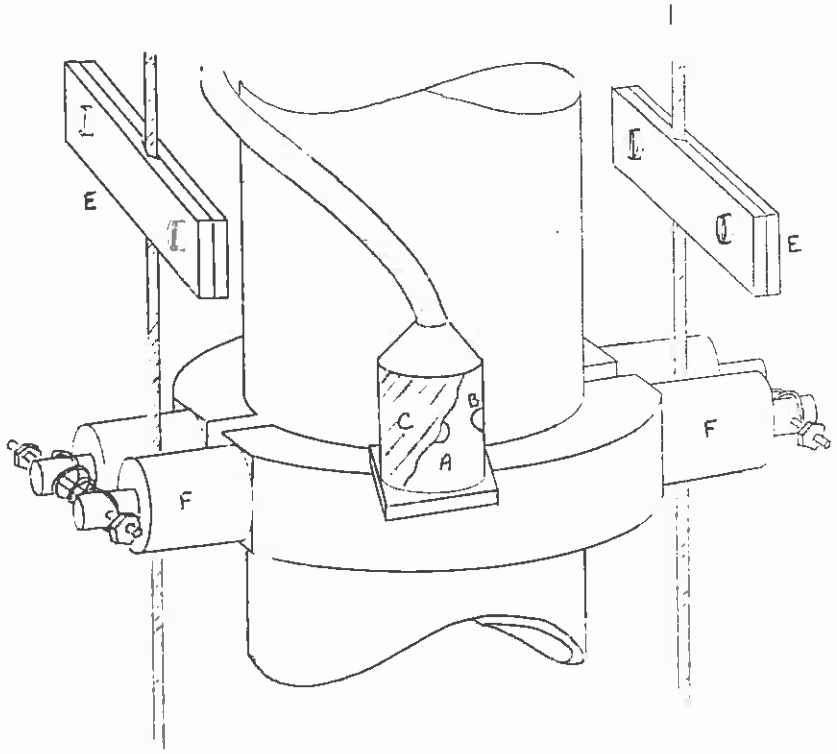

Fig. 15 Wave probe on the rod. A pressure transducer is placed in a housing, A. The openings, B , are covered with a rubber diaphragm, C (a bicycle inner tube). This housing are mounted on a collar which slides along the rod. When tide level is waning, the clamps, E , will hit the rollers, F , from time to time and force the collar deeper. The clamps shown are placed about 0.8 m below the water surface and two others about 1 m further down.

This could only be used for phase registrations, because the exact distance from probe to water surface was not known (an approximation could be obtained from knowledge about tide variations). The signal was used to compute the time to release the buoy. One drawback was that the dynamic pressure decreases with depth and significant waves might not be

registered if the collar was deeply submerged.

B. The pressure-probe rigs

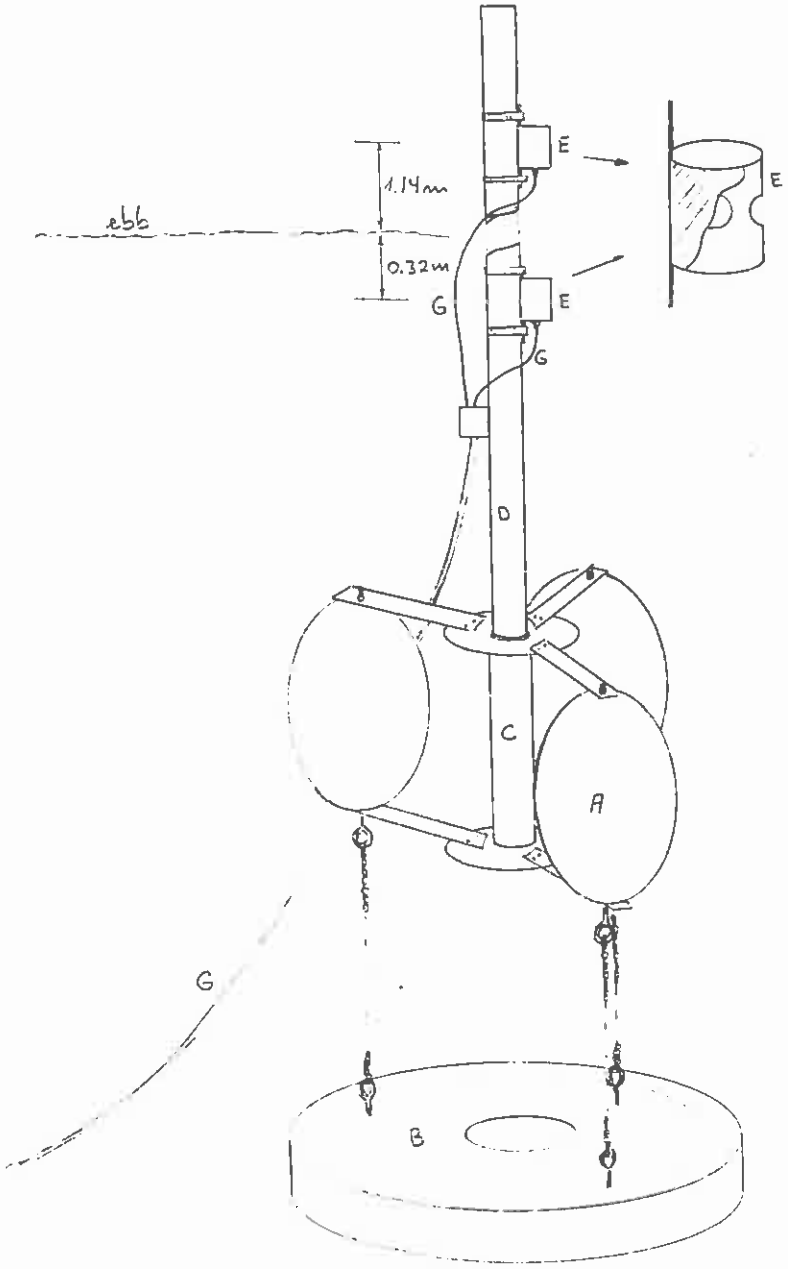

Fig. 16
The pressure probe rig is three floats, A , coupled in a triangel and chained to a railway wheel, B , on the sea bed. In the center of the triangel there is a casting, C , into which a rod, D , is thread. The rod is fitted with pressure transducers protected in small houses, E. F is a connection box and G cables.

There were two rigs placed beside the buoy (see C1 in fig. 2). As indicated in fig. 16, each rig had two probes to handle ebb and tide without getting to deep. The one used at high tide was above water level at ebb.

To avoid too much motion, the rigs were designed with a surging period differing from the wave period. Typical wave period was 2 - 3 s , and because of small stiffness in the

system, the surging period had to be longer than this. The actual period was approximately 6 s.

To do absolute wave measurements with these rigs, it was necessary to know tide level. Because of local weather situations tide tables does not always agree with realities. Therefore, two posts with scales were placed on the beach (fig. 17) so they could be read from the cabin window. Any way, the probes' calibration factors had to be corrected as tide level changed, so this was not a ready method.

Fig. 17 Posts with scale is a simple and safe way of measuring the tide level.

The signal from one of the riggs was used as control signal in period B and partly in period C because of a fault in the collar (4.1.A). However, the waves had both a frequency and a direction spectrum, so the delay from probe to buoy was very difficult to predict. It turned out that only a probe in the buoys position, i.e. on the rod or the buoy itself, would do. Even then it might be problems due to tilting and tide variations.

C. The float probes

The third type of wave probes did not require any knowledge about tide level, and it always measured the waves at the surface. The disadvantage was the necessity of

deep water. Fig. 18 shows the devise. Fig. 2, detail C2 shows the placing.

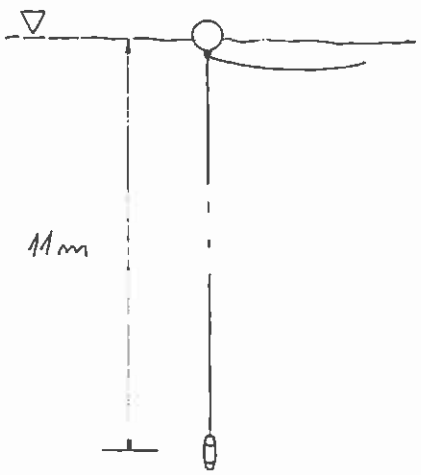

Fig. 18
Deep in the water, say more than half a wavelenght, the wave does not contribute to the pressure.
A torpedo-shaped housing,A ,with a pressure transducer is hanging in the electric cabel,B,from a float,C.
When the float follows the waves, the probe,A,also will and it therefore "sees" a variating pressure.

These probes were used to find the average wave climate. It was assumed that this was representative also for the wave climate at the position of the buoy.

4.2 Position and acceleration

To measure the buoy's motion in the rod direction, a potentiometer coupling was used, fig. 19.

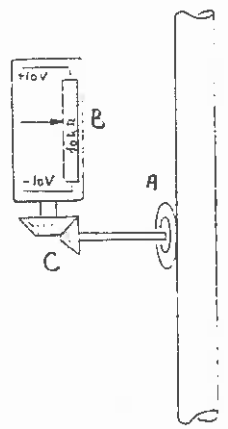

Fig. 19
The position transduder schematic.
A rubber wheel, A , is rolling on the rod and drives a 10-turn potentiometer, B , via a gear, C. The wheel, A , is pressed against the rod by springs.

The placing of the transducer is shown in fig. 7. The acceleration transducer is also indicated there. It was of the inductive type.

4.3 Chamber pressure

The pressure transducer used the same principle as the acceleration transducer, but this time a diaphragm was connected to the core. It was found that an acceleration of one g gave a fault of about 120 Pa in pressure measurements.

The placing is indicated in fig. 7. The diaphragm was protected with silicone grease. Once there was problems with moisture in the transducer, but it worked properly after drying, and a check showed no change in calibration factor.

4.4 Chamber level

Measurements of the water level inside the buoy turned out to be the most difficult problem to solve.

Two-wire resistanse probes seemed to be unfit because of sea water's high conductance and short circuit possibilities. Because of accelerations of the water column in the buoy the level could not be determined on the basis of pressure measurements in the water. Therefore, a capacitive transducer was designed. One electrode was a vertical wire about halfway submerged and insulated from the water by a dielectricum (plastics). The other electrode was the water itself.

The main problem was that water (especially sea water) stick to the dielectricum and a proper material was difficult to find. Finally a 0.3 mm insulated copper wire for coils was used. It worked, but got too delicate and was destroyed after a few days in sea, although it had worked for weeks in laboratory (in a tank with sea water). The wires was renewed once, but broke down again. Another problem was fouling of the wires, which after some time obscured the measurements. Fig. 19 shows the transducer. There were three sets of wires to get a avarage when the buoy tilted. The probe was used some days in period E.

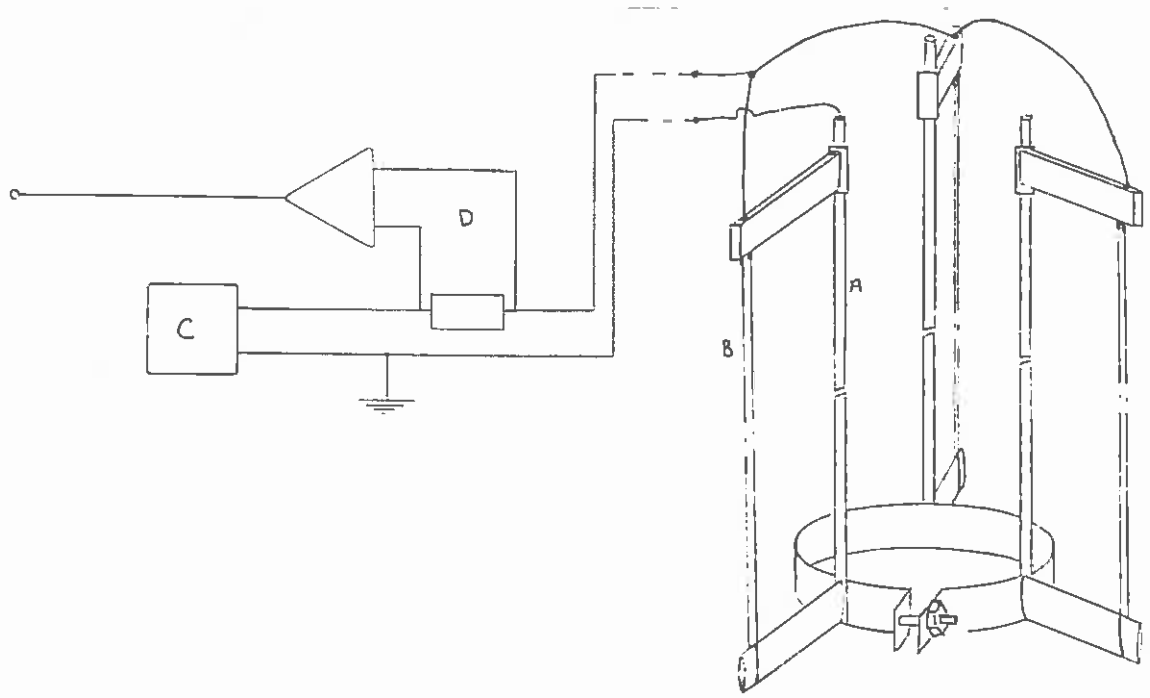

Fig. 19 Water level transducer. The brass rods, A , make electric connection to the water, and this is one electrode, the copper inside the insulated wires, B , is the other. The capacity of a cylinder capacitor is proportional to the cylinder length and hence to water level. A certain voltage, 10 kHz, is supplied, C , to the transducer and the current is measured, D. Schematic circuit diagram.

4.5 Friction forces

A considerable amount of absorbed energy was drained through friction against the rod and viscous losses. The first, which arised from guide rollers and latching mechanism, was measured by means of a load cell just above the anchor joint (fig. 13). The viscous losses could not be measured, but the results suggested that they were fairly large. See Ch. 6.3.d.

4.6 Forces on the guide rollers

Prior to period D the guide roller brackets on the buoy were fitted with strain gauges to measure the radial forces on the rollers. The coupling is shown in fig. 20.

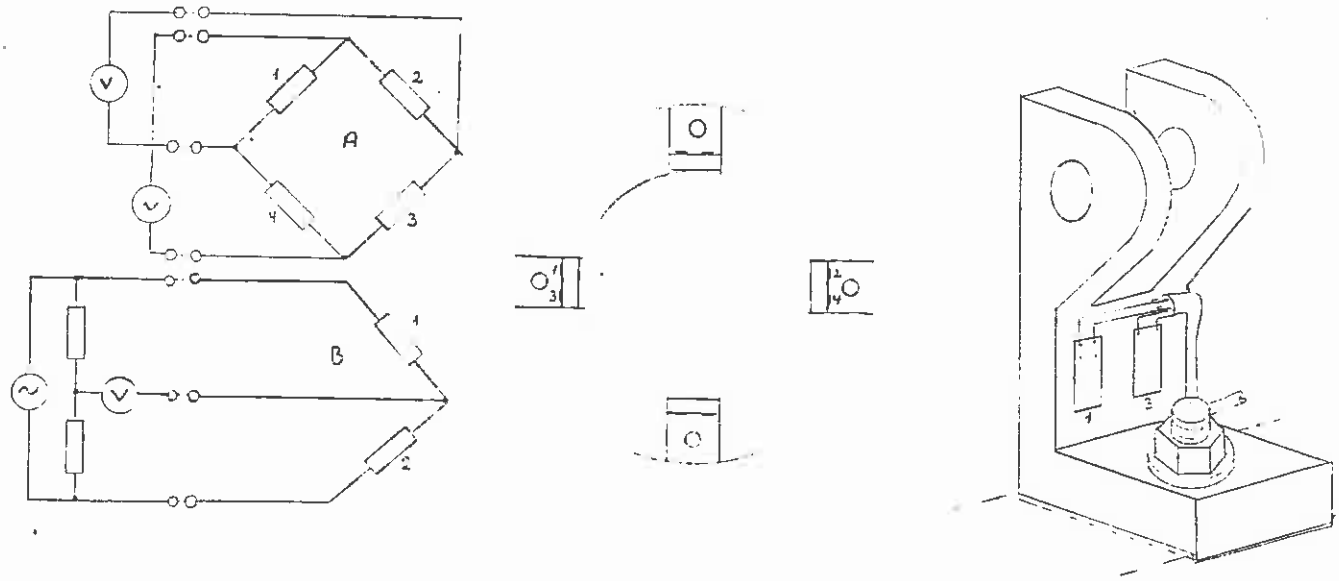

Fig. 20 Strain gauges registered forces on the guide rollers. On the upper roller ring they were coupled as a full bridge , A, one for each direction (X and Y). On the lower ring each bracket only had one strain gauge and they were couplet in half-bridge, B.

Measurements were not done before period E. One source to faults was that rotational movement of the buoy would apply a torque to the brackets which was registered as a radiell force. However, the measurements were only ment to give an idea about the size and not any exact values.

4.7 Electric cables

For measure signals only screen cables were used, and between the fleet and land most of them were protected in a soft PVC hose. The cables from the strain gauges on the guide roller supporting brackets were protected in another hose and connected only when measurements were to be done. There were three 220 V cables, one to each valve and one to the hydraulic pump.
The initial plan was to run out the cables, of a standard length of 100 m , directly from land to the buoy without any couplings between. However, after placing the buoy on the proper depth, it was discovered that the cables were too short. Extension cables were necessary, and the fleet was fitted with a connection box. Later experiences showed that this was necessary also for other reasons. Primarally, the fleet acted as tension relief and the connection box as checkpoint. Secondly, when putting the buoy into sea, the extension cables were connected to the buoy in advance, and the coupling to the cables from land was done on the fleet. This was an advantage. In addition, the extension cables were not put into a hose. Then they got lighter and more flexible, and the buoy was less affected by them. For the wave probes (except the collar) special waterproof cables were hauled to the pressure-probe riggs and to the mooring buoy (C1 and D1 in fig. 2) and there connected to minor cables from the transducers (see fig. 16).

5. PHASE CONTROL

5.1 Releasing the buoy

Wave prediction was achieved by using the Kalman filtering technique as described in [1] and [5]. More details are given in Appendix A. During the registration periods B, D and E the control signal was taken from a pressure probe at the rod. During the registration period C the control signal was taken from a pressure probe attached to a rigg standing a couple of meters away from the buoy.

When the control signal is measured at the rod the tilting of the buoy and the tidal variation will result in a fluctuation in the mean signal level due to the variation of the hydrostatic pressure. If the fluctuation is significantly slower than the typical wave period as is the case for the tidal variation, it can be compensated for by using the mean level as an extra variable in the Kalman filter. This is shown in [5]. In regard to tilting the experiments showed that at many times it was difficult to compensate for this. The problem of tilting is discussed in more detail in Chapter 6.1.

When the control signal was measured away from the buoy a mean time difference between the probe and the buoy was stipulated and then used in the prediction program. The experiments showed that this method worked only if the spectrum of the incident wave is narrow both in frequency and direction. Further, tilting will also here represent a serious problem, especially if the buoy tilts in the same direction as the incident wave.

5.2 Latching the buoy

The latching mechanism has to be prepared for latching just ahead of the time when the buoy has reached its top or bottom.

This is achieved by measuring both the velocity and the acceleration of the buoy. The two signals are added together. When zero crossing in the resultant is detected the latching mechanism is prepared for latching. By adjusting the amplification of the acceleration signal it is possible to tune this zero-crossing so that the latching mechanism functions properly with a minimum of frictions losses. A special electronic unit 'BØY-TØY' has been made for this purpose. The principle is shown in fig. 21.

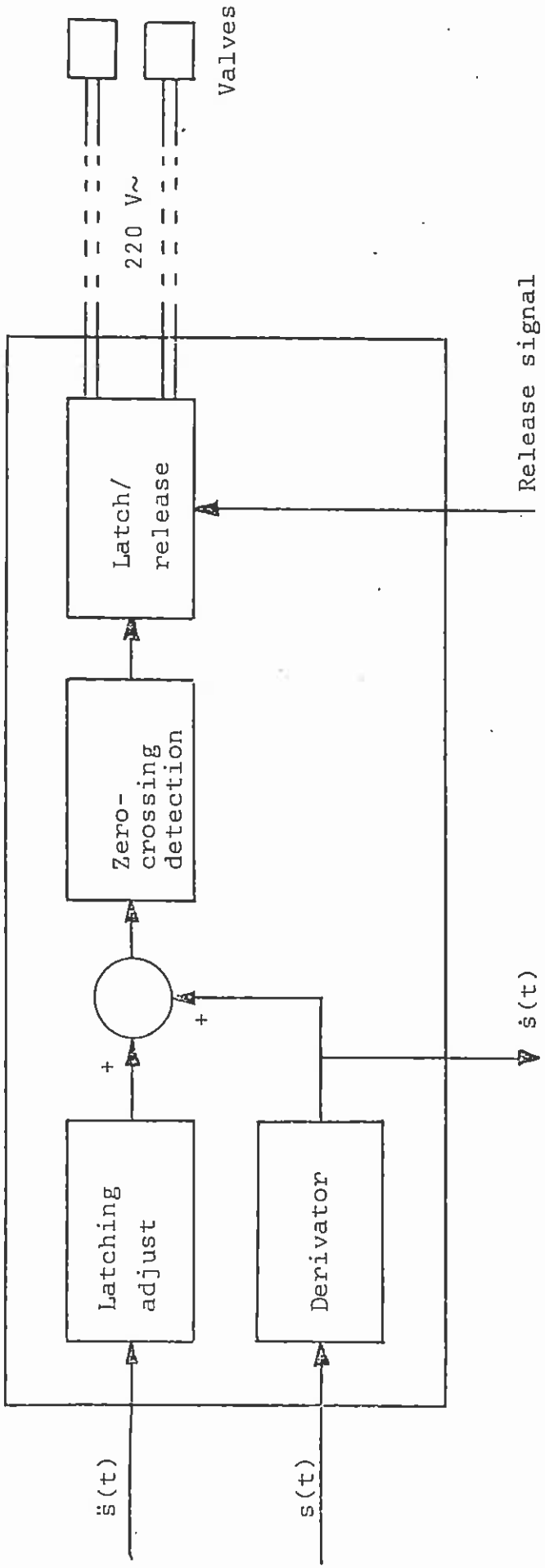

Fig. 21 The 'BØY-TØY' unit used for preparing the latching mechanism. The velocity of the buoy is obtained by derivating the measured position.

6. EXPERIMENTAL RESULTS

All registrations refered to in this chapter are taken from the testing period E.

6.1 Phase control

Fig. 22, 23 and 24 show three different registrations. The position of the buoy is shown together with the incident wave. In addition, the measured frequency spectrum of the incident wave is shown together with an analytical JONSWAP spectrum having the same significant height, H_s , and zero upcrossing period, T_z , as the measured wave. Fig. 22 shows a registration where the buoy oscillates quite constantly during the whole registration period. This is, however, not a typical situation and Figs. 23 and 24 are more representative for what was achieved most of the time.

Phase control has earlier been tested in a wave channel with plane, irregular waves having a narrow spectrum [1], [6]. These experiments have shown that in such a situation it is possible to achieve a quite satisfactory phase control with the present Kalman filtering technique. In the experiments in Trondheimsfjorden it is more difficult to obtain good phase control due to the following reasons:

a) The combination of wind generated waves and swells gives a broadening and also at some times a two-peaked frequency spectrum. Fig. 23 shows a situation with a broad spectrum.

b) By visual observation it is seen that the directional spectrum at many times is rather broad or multi-peaked. This makes phase control more difficult.

c) The typical wave period in Trondheimsfjorden was found at most times to be somewhat small compared to the 1:10 scale.

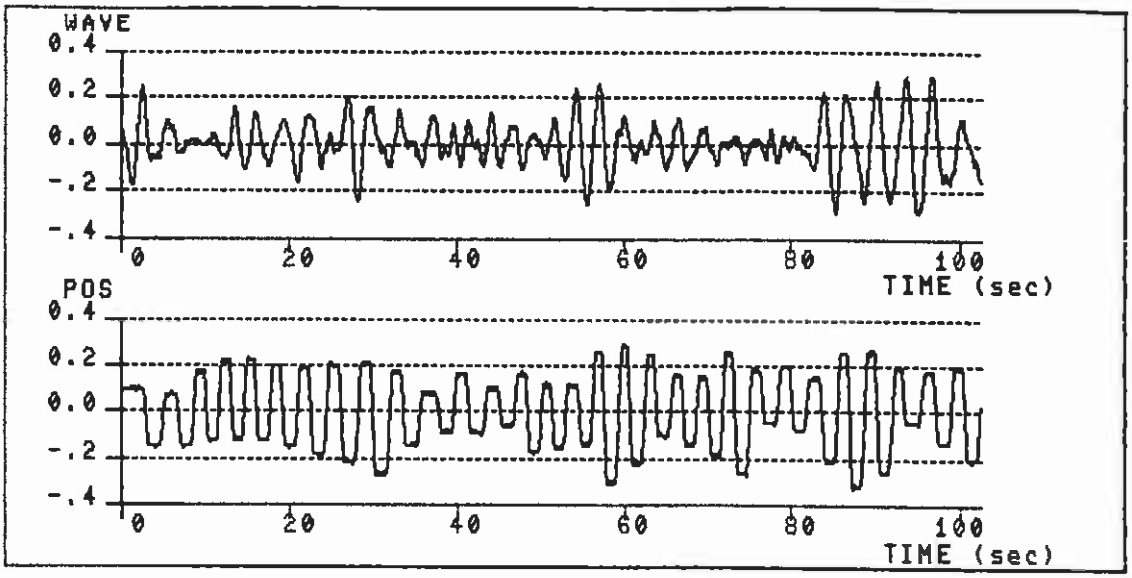

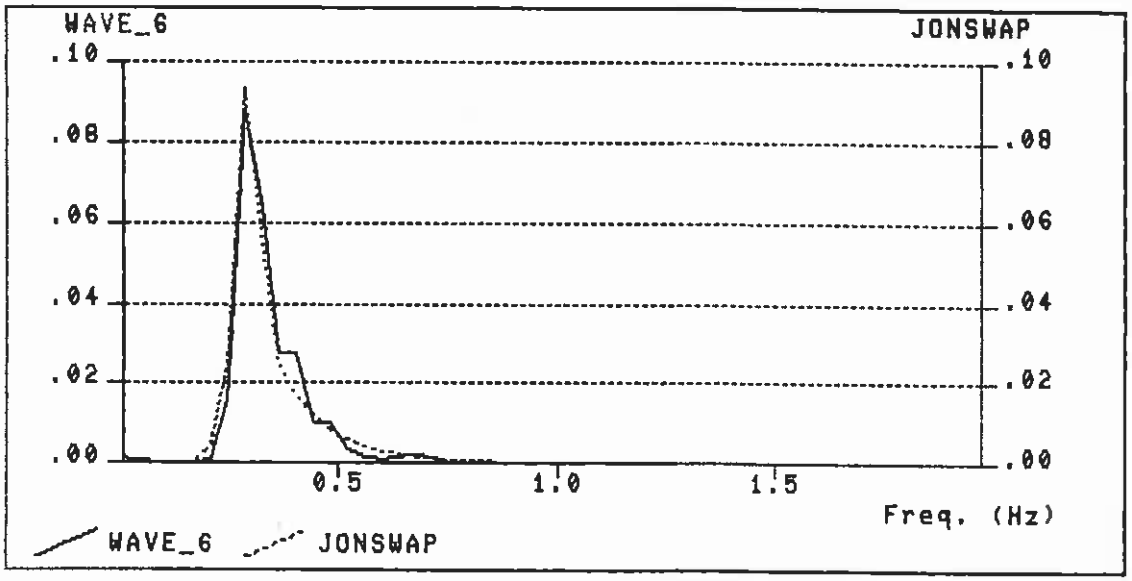

Fig. 22 Reg. no. 8. The buoy oscillated quite constantly. The JONSWAP spectrum is used with $\gamma = 3.0$

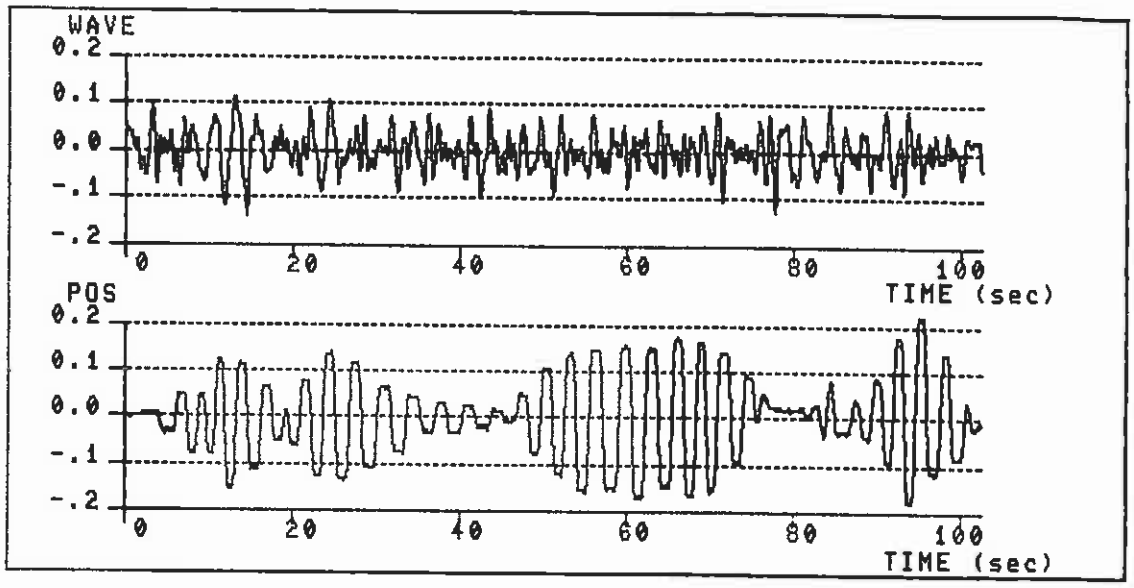

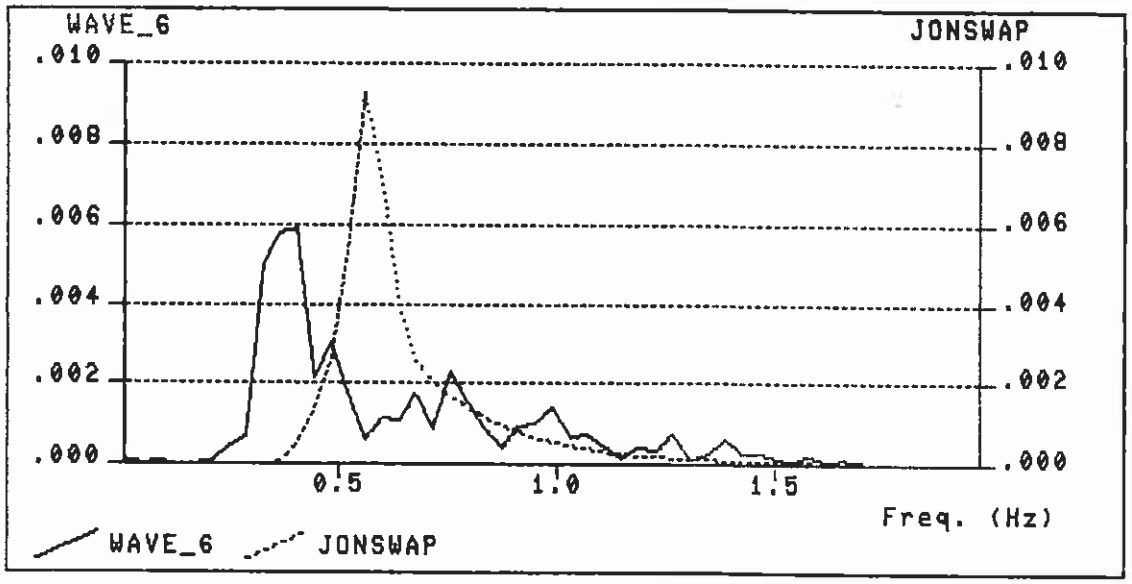

Fig. 23 Reg. no. 32. The oscillation of the buoy is not stable. The JONSWAP spectrum is used with $\gamma = 3.0$

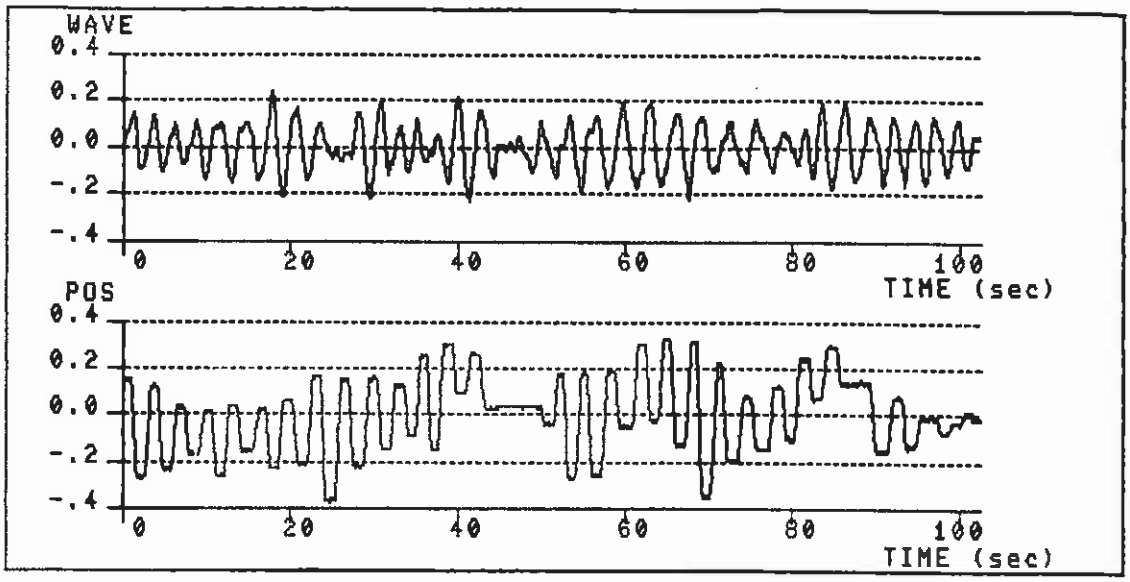

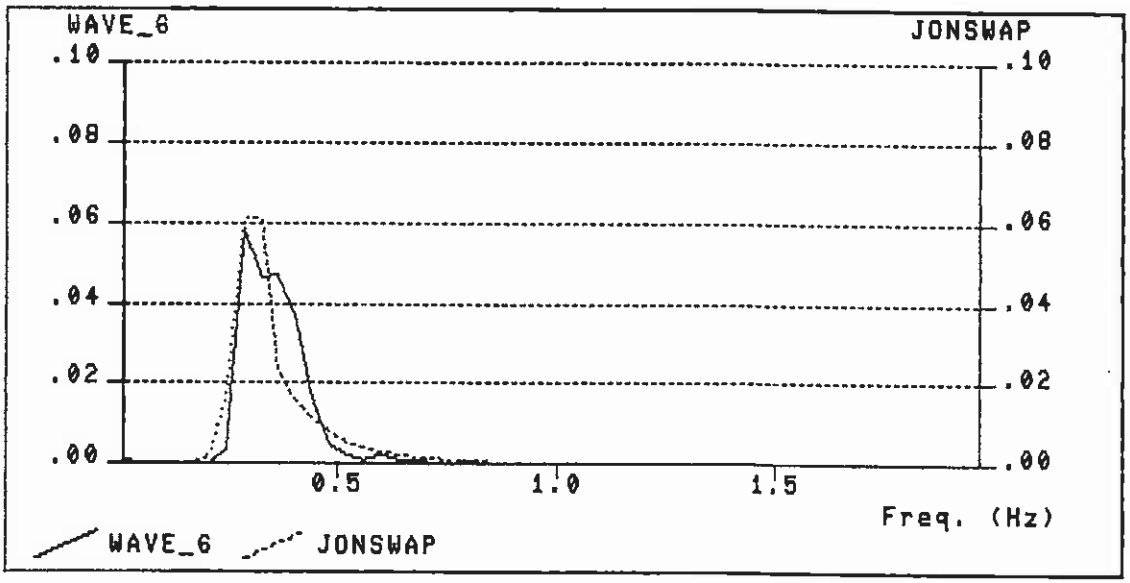

Fig. 24 Reg. no. 9. The buoy has a tendency to tilt. The JONSWAP spectrum is used with $\gamma = 3.0$

Most of the time T_z was found to be below 2.0 sec. This is too close to the natural period of the buoy, T_b = 1.5 sec, to expect good phase control.

d) The control signal was measured by a transducer at the rod. The depth of submergence of this transducer varied during the ebb and tide syclus. Especially before and at high tide this depth was rather large, approximately 1.8 m. If the spectrum is broad the higher frequency components of the wave may then be filtered so much that the control signal gives a poor representation of the excitation force on the buoy.

e) The buoy has a tendency to tilt due to the pressure from waves, wind and current. This tilting can be extra large when the buoy is phase controlled. When the buoy is latched in its upper position the resistance against tilting is much smaller than the resistance against restoring when the buoy is latched in its lower position. The tilting of the buoy results in a hydrostatic drift in the control signal. This drift can be difficult to compensate for. In addition, as a result of tilting the buoy looses height. Fig. 24 shows a registration where tilting two times almost completely destroys the oscillation. Note that a full scale buoy has a larger stability against tilting than the model buoy. The counter mass at the rod is too light and its depth of submergence is too small for the model buoy. Further, in the model experiments in Trondheimsfjorden the rod has to be extraordinary long due to the large tidal range. In addition, a stopping mechanism with a certain weight is used at the top of the rod. All these factors contribute in reducing the stability against tilting.

6.2 The buoy motion

The buoy can be operated in 3 different modes - free, latched and controlled. In this section it will be discussed how the internal water level, s_i , and the chamber pressure, p_c , vary in detail for each of the 3 different modes.

a) The buoy is free - cf. fig. 25.

Both s_i and p_c are almost constant

b) The buoy is latched - cf. fig. 26.

The zero crossing of p_c is almost in phase with the zero crossing of the incident wave. The phase difference between the maximum of p_c and the maximum of the incident wave is due to the air flow through the orifice. The phase difference between s_i and the incident wave is approximately 80^o in this particular example.

c) The buoy is phase controlled - cf. fig. 27.

When the buoy is released from its lower position the chamber pressure drops quickly to a level around the atmospheric pressure. The minimum is reached after 0.3 sec. The internal water level drops a little and this variation is at its largest when the buoy has its largest velocity. When the buoy is retarded the internal water level increases again and the same is observed for the chamber pressure at the last part of the stroke.

When the buoy is latched in its upper position the chamber pressure again drops quickly. The lowest value is reached after approximately 0.4 sec. Then the pressure increases due to the airflow through the orifice. While the buoy is latched the internal water level drops with a rather constant velocity down to its lowest level.

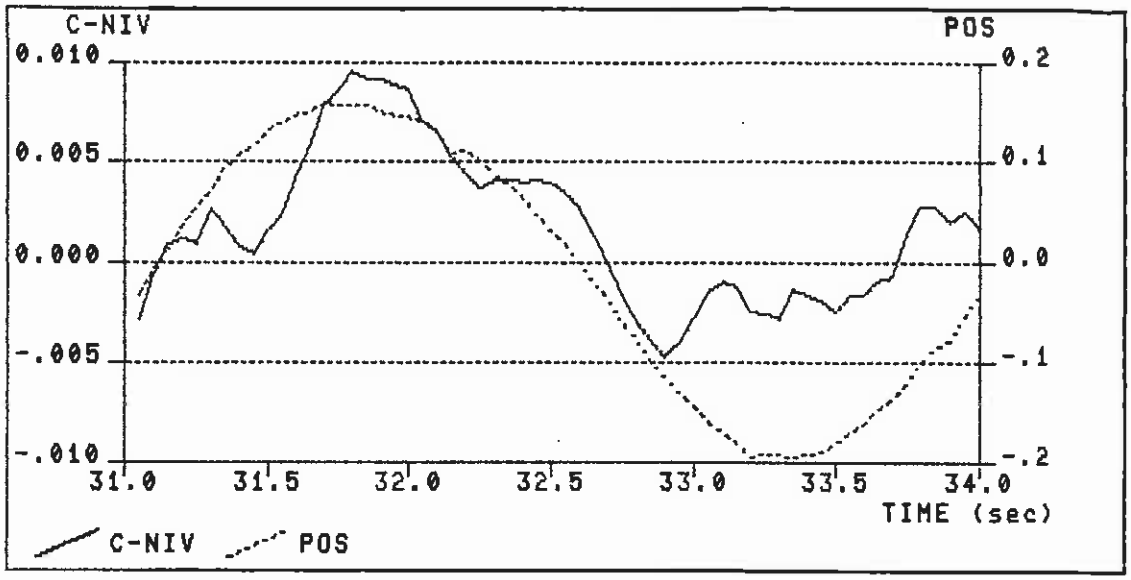

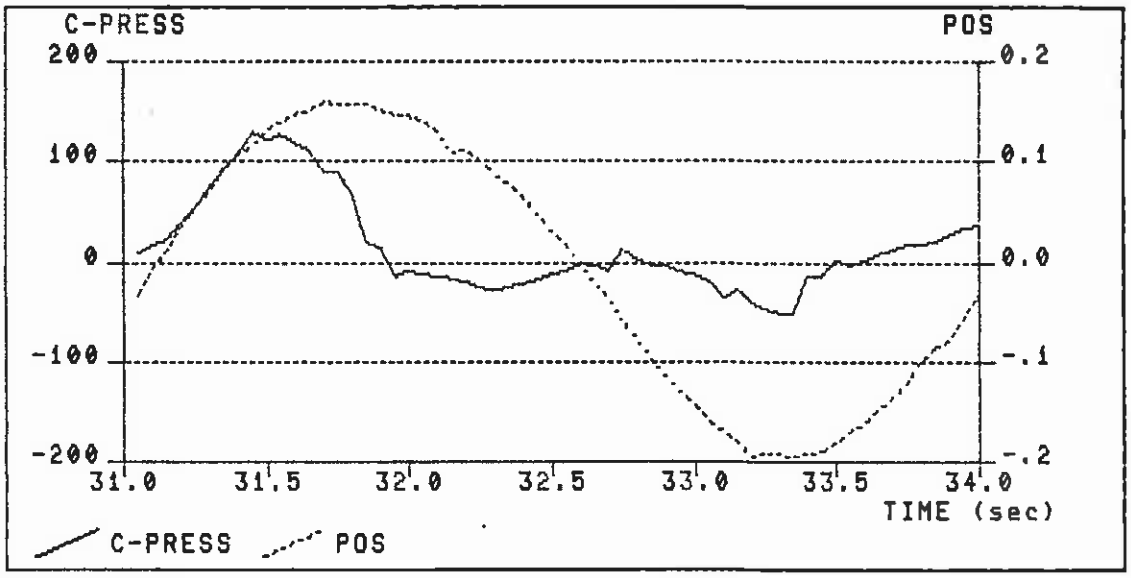

Fig. 25 Reg. no. 6. The buoy moves freely.
C-NIV: The internal water level.
C-PRESS: The chamber pressure.
POS: The position of the buoy.

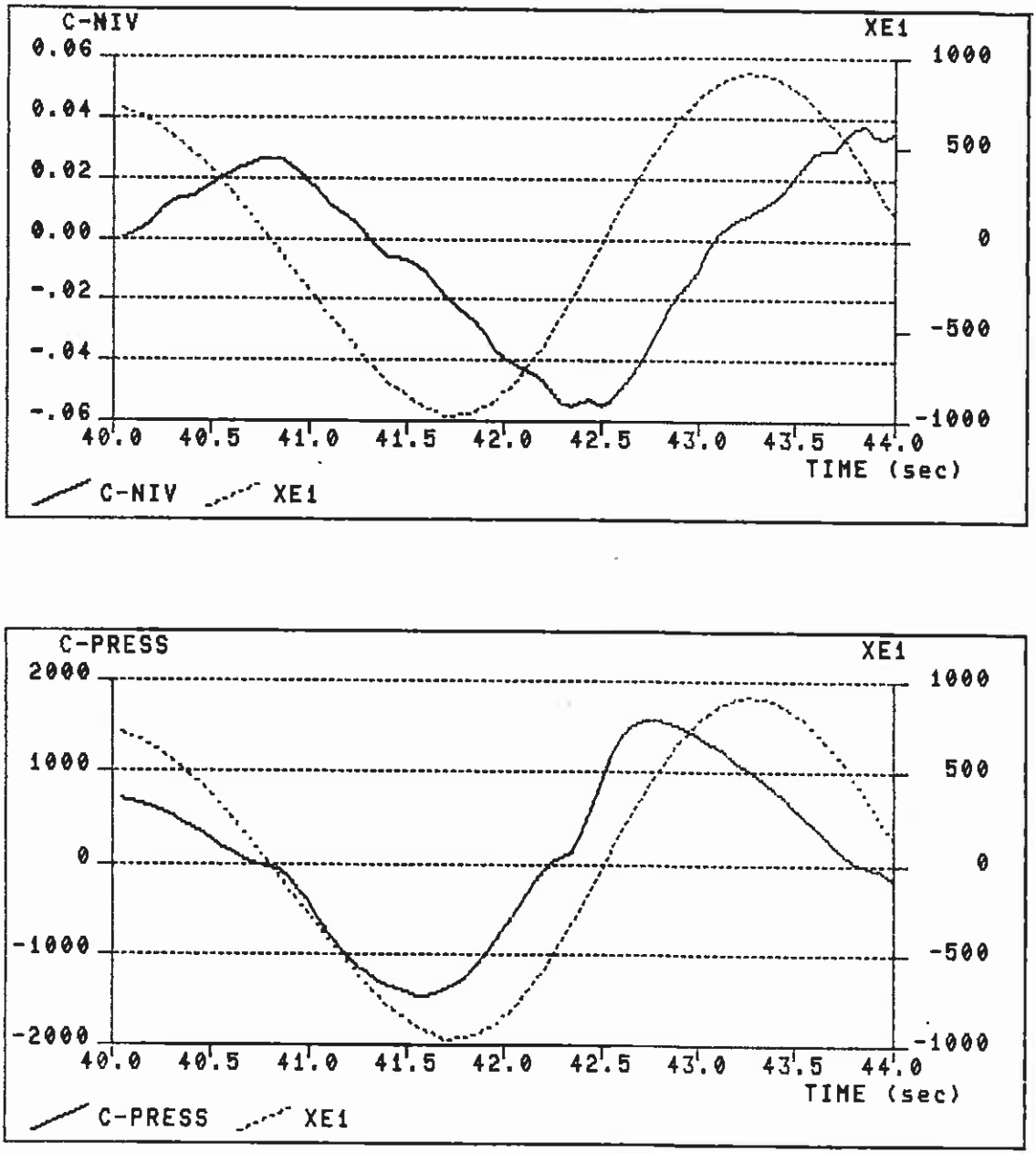

Fig. 26 Reg. no. 7. The buoy is latched.
XE1: The pressure at the rod. The measured signal is Kalman filtered.

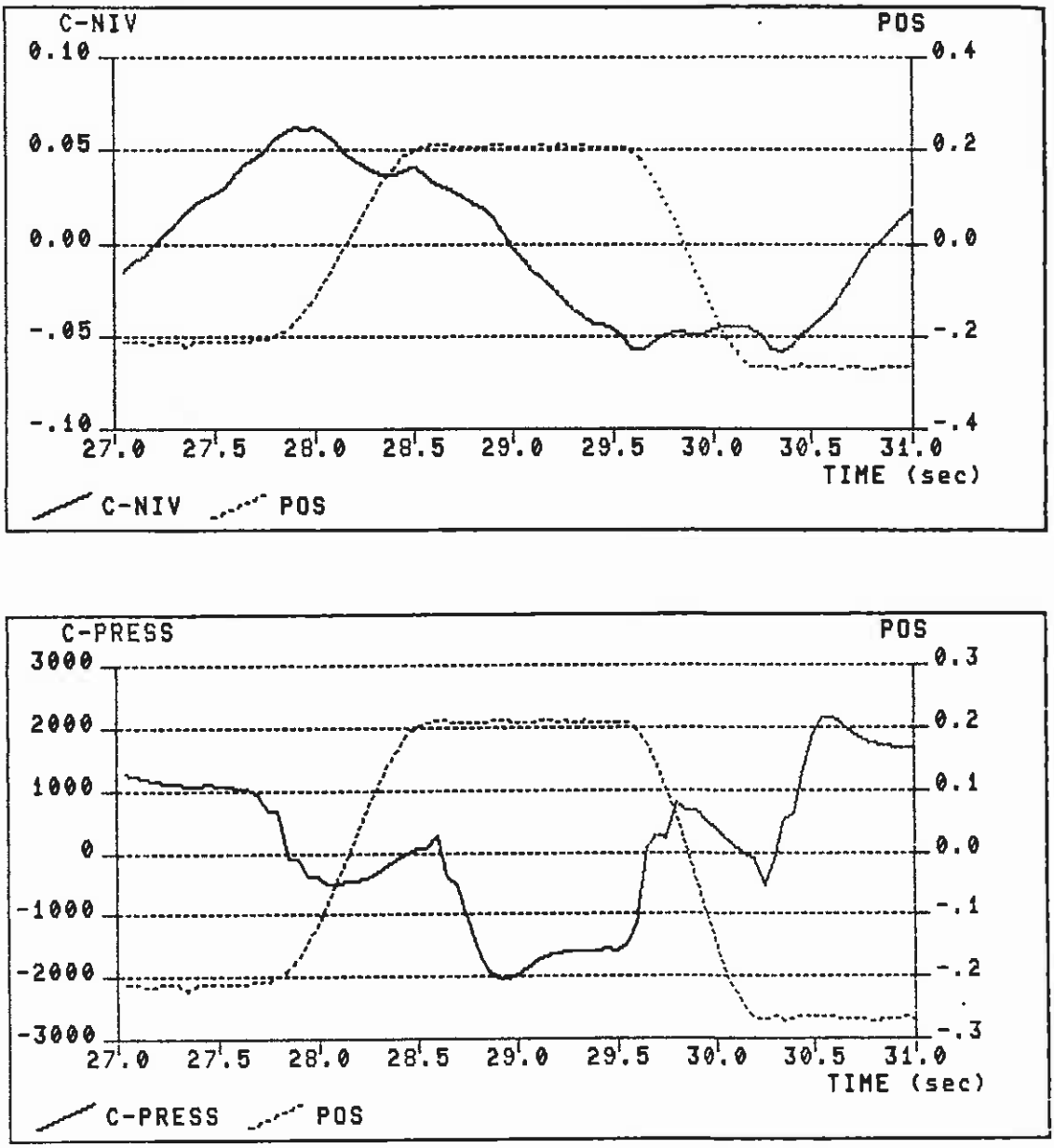

Fig. 27 Reg. no. 8. The buoy is phase controlled.

Note that almost all the pneumatic energy is produced during the time when the buoy is latched.

6.3 Energy absorption

Among all the registrations altogether 12 time segments (from t_1 to t_2) have been picked out and analysed in more detail. These time segments are chosen where the oscillation of the buoy was as constant as possible. Further, the length of each segment is chosen so that the segment contains a whole number of buoy periods.

a) Friction power

The friction energy loss, E_f , is found by using

$$E_f = \int_{t_1}^{t_2} F_z(t) \left(\frac{ds}{dt}\right) dt \qquad (1)$$

where F_z is the rod force and s is the buoy position relative to the rod. The mean friction power is

$$P_f = \frac{E_f}{t_2 - t_1} \qquad (2)$$

During the time segment being studied the buoy moves a total distance s_{tot} . The mean friction force is then defined as

$$F_f = E_f / s_{tot} \qquad (3)$$

For the 12 time segments being studied the mean friction force is found to be $F_f = 52 \pm 5$ N. In comparison, when the buoy moves freely the corresponding value is found to be 12 N.

b) Pneumatic power

There are two methods for finding the pneumatic energy, E_p. Method 1 is to use the calibrated orifice. The orifice is calibrated in a steady flow [4]. The pneumatic energy is found as

$$E_p^{(1)} = \int_{t_1}^{t_2} C_o(p_c(t))\, dt \qquad (4)$$

where $C_o(p_c)$ is the calibration function for the orifice.

Method 2 is to use the internal water level together with the chamber pressure

$$E_p^{(2)} = A_i \int_{t_1}^{t_2} p_c(t)\left(\frac{ds_i}{dt}\right) dt \qquad (5)$$

where A_i is the internal water plane area.

In only 5 out of the 12 chosen time segments the measuring of s_i functioned properly. For these 5 segments it is found that $E_p^{(2)} \approx 0.6\ E_p^{(1)}$. In the following Method 1 is used since this method is based upon measuring only the chamber pressure which is done very accurately. The measurement of the internal water level is much more dubious.

The mean pneumatic power is found as

$$P_p = \frac{E_p}{t_2 - t_1} \qquad (6)$$

c) Absorbed power compared with theory

The pneumatic power plus the friction power is denoted as the absorbed power, P_a . The absorbed power should be compared with the theoretical estimate, P_t. The theory being used here assumes a semi-submerged sphere being phase controlled in a regular sea. The theory is presented in more detail in Appendix B . In the present case the waves are, however, not regular. Moreover, the sphere is not complete and the system has an additional degree of freedom because of the internal water column. The problem with irregular waves are partly overcome by selecting time segments where the buoy motion is as regular as possible. Further, it is assumed that the deviation in shape from a complete sphere and small motion of the water column will not affect the power absorption to any great extent compared with that for the complete sphere. One should however remember that the validity of these assumptions is not proven.

As shown in Appendix B the theoretical power absorption can be expressed by the following 5 quantities

T_o - The wave period
T_b - The natural period of the buoy
η_o - The wave amplitude
s_m - The stroke amplitude of the buoy
φ - The phase angle between the excitation force and the velocity of the buoy.

Based upon the measured signals these 5 quantities are found as follows

$$T_o = \frac{t_2 - t_1}{n_s} \qquad (7)$$

where n_s is the number of strokes during the time segment.

The buoy period is assumed to be T_b = 1.5 sec. The wave amplitude is found by using the significant wave height for 512 data points (= 25.6 sec.) including the time segment being studied.

$$\eta_o = \frac{1}{\sqrt{2}} \frac{H_s}{2} \tag{8}$$

The stroke amplitude is found as

$$s_m = \frac{s_{tot}}{4n_s} \tag{9}$$

An analyse program 'PHASE' is used in order to obtain a quantitative estimate, α , on how good the phase control is [6]. The mean phase angle is then assumed to be

$$\varphi = \cos^{-1}(\alpha) \tag{10}$$

Among these 5 quantities the wave amplitude, η_o , is the one with the largest uncertainty. This uncertainty is mainly due to the fact that the wave is measured away from the buoy itself (approximately 40 meters).

Tabel 1 and fig. 28 show P_a compared with P_t for the 12 time segments. For very small power levels the agreement between the two is satisfactory. But for higher power levels P_a is much smaller than P_t . As already pointed out it is a large uncertainty in P_t due to the method being used for finding the wave amplitude. Still, the difference between P_a and P_t is absolutely significant.

Reg. no.	$t_1 - t_2$	n_s	T_o(s)	η_o(m)	s_m(m)	φ	P_p(W)	P_f(W)	P_a(W)	P_t(W)
8	10-30	12	3.3	0.11	0.18	20^o	49	9	58	105
9	20-30	6	3.3	0.13	0.19	20^o	56	12	68	133
16	26-43	10	3.4	0.10	0.19	10^o	53	11	64	102
16	80-100	12	3.3	0.09	0.21	14^o	59	15	74	97
30	30-41	8	2.8	0.04	0.13	10^o	20	10	30	23
31	0-18	14	2.6	0.04	0.06	9^o	5	5	10	14
32	50-71	14	3.0	0.04	0.15	0^o	21	9	30	27
46	85.5-97	8	2.9	0.10	0.11	8^o	15	8	23	67
50	61-78	10	3.4	0.11	0.24	0^o	42	16	58	141
53	51-68	12	2.8	0.14	0.22	16^o	33	16	49	172
55	60.3-79.1	12	3.1	0.12	0.19	11^o	34	14	48	130
56	59-69	10	2.0	0.05	0.12	0^o	13	13	26	19

Table 1 The measured power absorption, $P_a = P_f + P_p$, compared to the theoretical estimate, P_t, for the 12 chosen time segments. The 4 quantities T_o, η_o, S_m and φ are also shown. These quantities are used when computing P_t as shown in Appendix B.

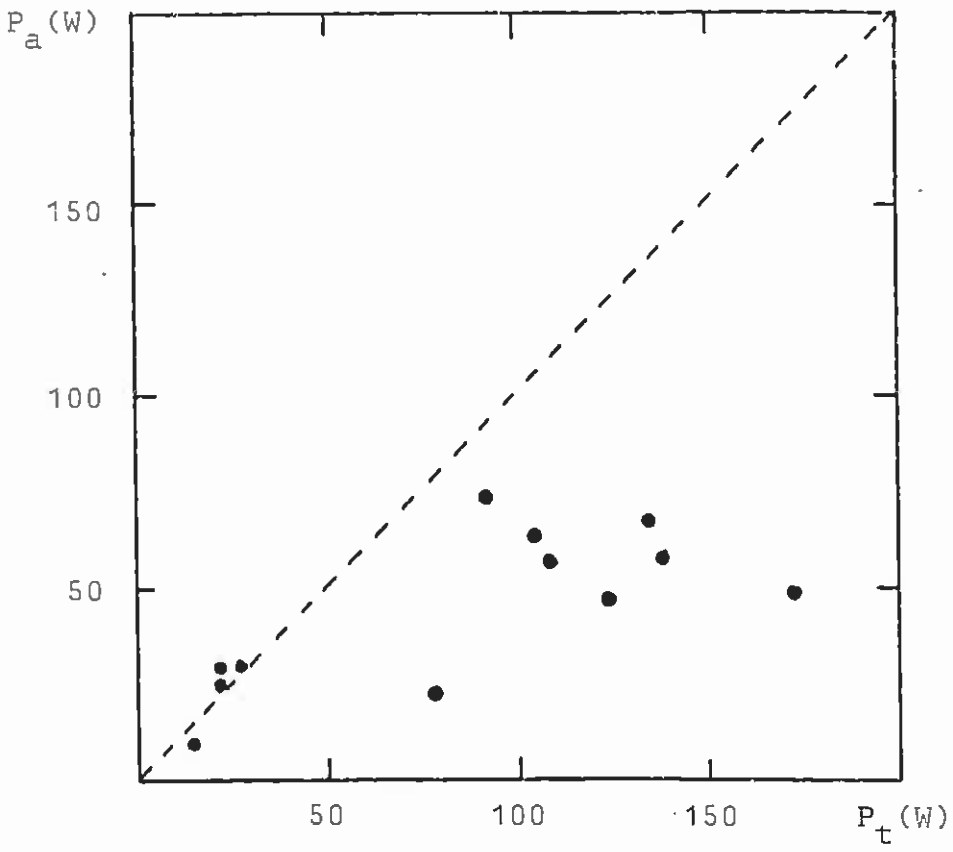

Fig. 28 The absorbed power, P_a , compared to the theoretical estimate, P_t.

d) The oscillation of the water column

The most obvious reason for the deviation between P_a and P_t is large viscous eddy losses because of the oscillation of the water column. In the following it will be shown that this oscillation is so large that one should expect large eddy losses. Fig. 29 shows the oscillation amplitude, s_i, of the water column as a function of P_p. Note that if the calibrated orifice gives a correct measurement of P_p the correct value for s_i is approximately 1.7 times the measured value. In fig. 29 the measured value is used but this should then be a very conservative estimate for s_i. The internal water plane area i $A_i = 0.41\ m^2$ whereas the area at the outlet is only $A_u = 0.13\ m^2$ which means $A_i/A_u = 3.1$. In addition, the real outlet is somewhat smaller because of the lower bearings. It is therefore assumed that the amplitude at the outlet is $s_u = 3.3\ s_i$. In fig. 29 this is used to get the s_u-scale.

Knott and Flower [7] has studied viscous losses in a oscillating water column as shown in fig. 30A. One conclusion is that the eddy losses are small as long as $s_i/r < 5$ where r is the radius of curvature at the outlet. The shape of the model buoy is shown in fig. 30B. For the model buoy the streamlines at the outlet converge towards the axis of the buoy whereas they diverge for the buoy with vertical walls. One should therefore expect the model buoy to represent a less favourable shape in respect to eddy losses. In addition, it is already pointed out that the estimate for s_i and s_u are very conservative. Still, fig. 29 shows s_u to be 0.15-0.20 m when $P_p \approx 50\ W$. The radius of curvature is $r = 0.025\ m$ which means $s_u/r \approx 6\text{-}8$. The conclusion is therefore that it is reasonable to suspect that a substantial amount of power is lost in eddies being generated at the outlet of the water column.

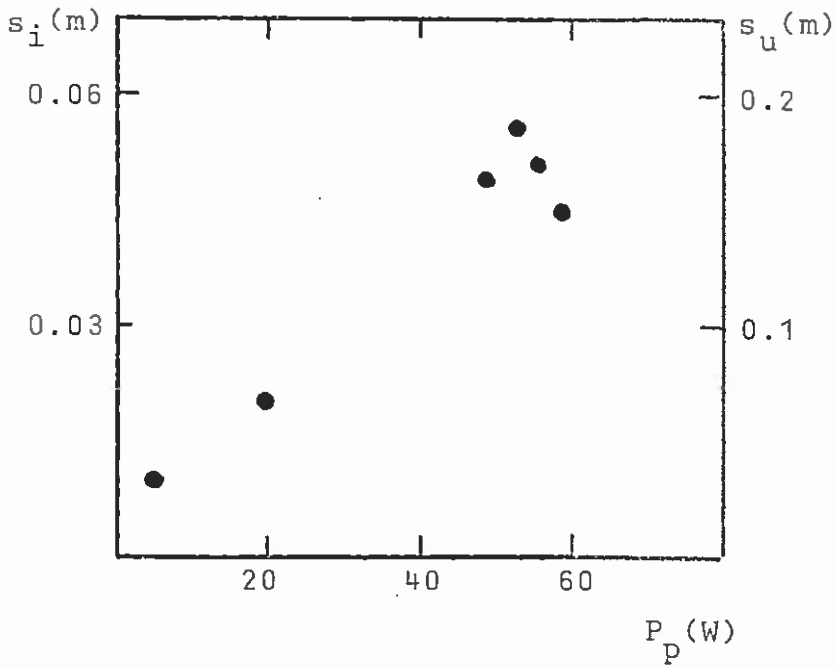

Fig. 29 The oscillation amplitude of the internal water level, s_i, and the oscillation amplitude at the outlet of the buoy, s_u, as a function of the pneumatic power, P_p.

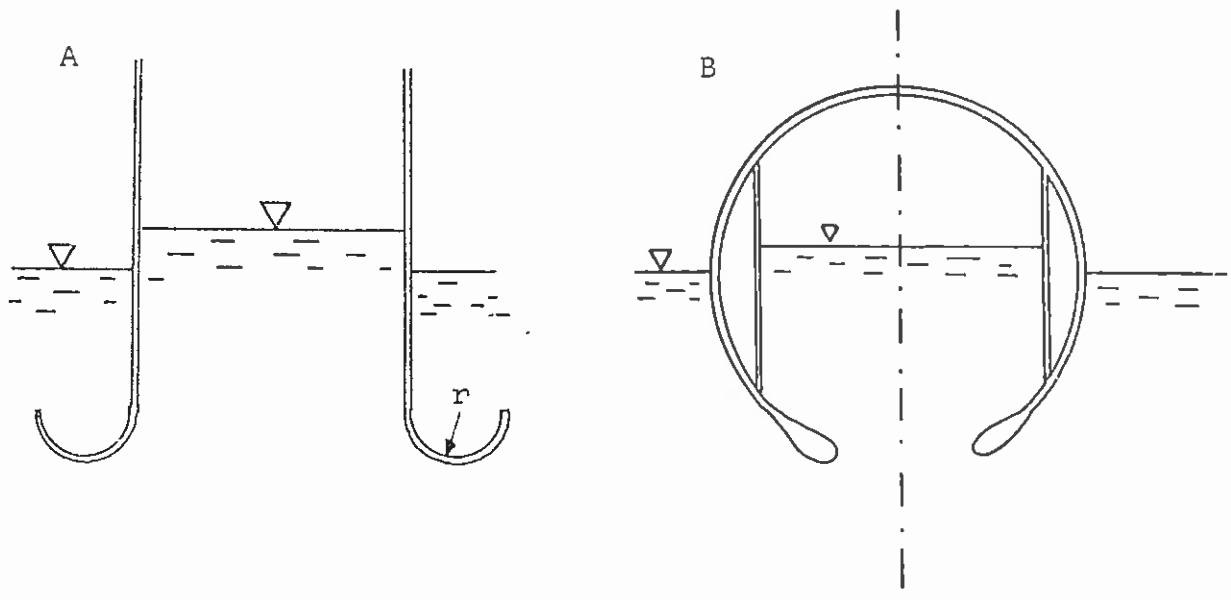

Fig. 30 Fig. A) shows the shape of the oscillating water column being studied by Knott and Flower [7].
Fig. B) shows the shape of the N2-model buoy.

e) Controlled motion compared to free or buoy

It may be of interest to compare the energy absorption for the three different modes of operation - free, latched and controlled. Table 2 shows such a comparison. The absorbed power is compared to the mean incident power pr. unit crest length, P_{in}.

$$P_{in} = \frac{\rho g^2}{64\pi} H_s^2 T_{-1} \qquad (11)$$

The difference between the free and the latched buoy illustrates the importance of having a fixed reference which in this case is the rod. The difference between the latched and the phase controlled buoy illustrates the importance of controlled motion. Note that the difference between these two modes of operation would be yet more significant if it had not been for the large viscous losses as discussed earlier.

6.4 Bearing forces

The dynamic bearing forces have been measured in the 3 different modes of operation. An example is shown in fig. 31. Of special interest is the maximum bearing force amplitude , F_b . First the quantity F_b' is found in both x and y direction:

$$F_b' = 0.5(F_{max} - F_{min}) \qquad (12)$$

where F_{max} is the maximum value of the bearing force during the registration period and F_{min} is the minimum value. The bearing force amplitude is then defined as

$$F_b = \sqrt{F_{b,x}'^2 + F_{b,y}'^2} \qquad (13)$$

Reg. no.	6	7	8
Mode	Free	Latched	Controlled
T_z (s)	2.3	2.6	2.7
T_{-1} (s)	2.7	2.9	3.1
H_s (m)	0.27	0.35	0.36
P_{in} (W/m)	94	170	192
P_a (W)	2	18	47
P_{in}/P_a (m)	0.02	0.11	0.26

Table 2 Power absorption in the 3 different modes of operation - free, latched and controlled.

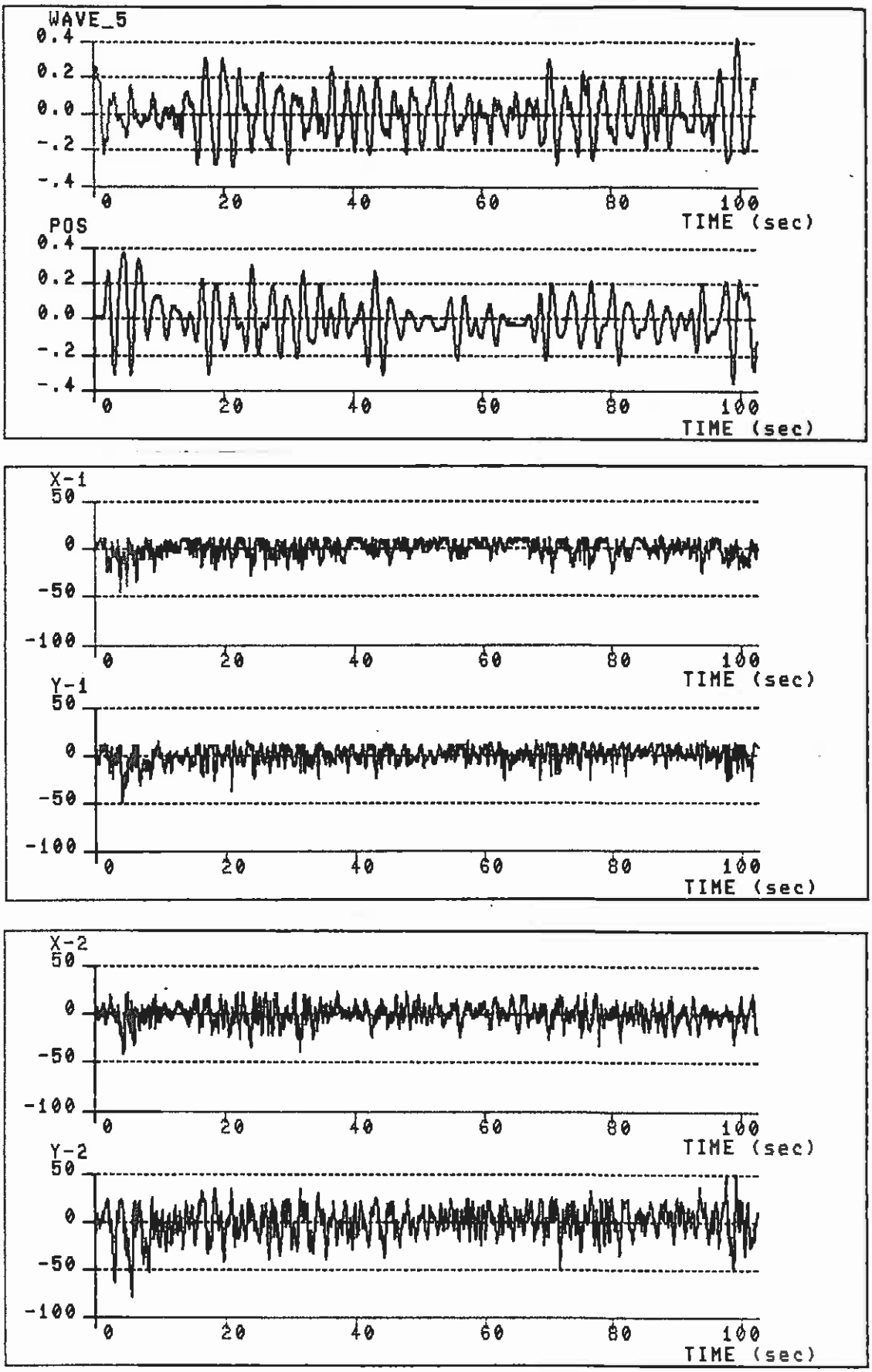

Fig. 31 Reg. no. 74. The bearing forces when the buoy moves freely.

X1 - Upper bearing forces in x-direction.

Y1 - Upper bearing forces in y-direction.

X2 - Lower bearing forces in x-direction.

Y2 - Lower bearing forces in y-direction.

Fig. 32 shows F_b for both the upper and lower bearings when the buoy moves freely. The wave period is T_z = 2.0-2.2 sec.

As seen in fig. 32 there is no typical trend to be observed as H_s increases. The bearing force amplitude is well below 100 N for all the 4 registrations shown. Note, however, that the yaw motion of the buoy can be rather large (± 15° typically). This yaw motion may influence the signal from the strain gauges measuring the bearing forces.

When the buoy is latched or controlled the latching mechanism will reduce the upper bearing forces. The forces in the lower bearings are similar to that for the free buoy.

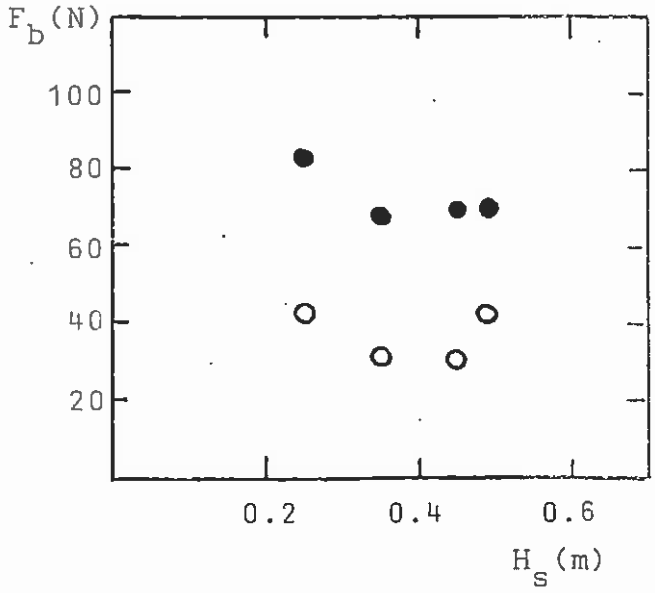

Fig. 32 The maximum bearing force amplitude, F_b, as a function of H_s for sea states with T_z = 2.0 - 2.2 sec.
Δ - Upper bearings.
▲ - Lower bearings.

APPENDIX A. KALMAN FILTER AND WAVE PREDICTION

One should refer to [1] and [5] for more detailed discussion. The same notation as in [5] is used.

Innovation when p_m is the measured control signal

$$\varepsilon = p_m - \bar{p}_1 \tag{A1}$$

A posteriori estimates

$$\left.\begin{aligned} \hat{p}_1 &= \bar{p}_1 + K_1\varepsilon \\ \hat{p}_2 &= \bar{p}_1 + K_2\varepsilon \\ \hat{\omega} &= \bar{\omega} + K_3\varepsilon \\ \hat{p}_\ell &= \bar{p}_\ell + K_4\varepsilon \end{aligned}\right\} \tag{A2}$$

Gain factors

$$\left.\begin{aligned} K_1 &= K_{1,0}\,\Delta t \\ K_2 &= K_{2,0}\,\omega_m{}^2\Delta t \\ K_3 &= K_{3,0}\,\hat{\omega}\Delta t \left\{\frac{K_1\hat{p}_2 - K_2\hat{p}_1}{(K_1{}^2\hat{\omega}^2 + K_2{}^2)p_a{}^2}\right\} \\ K_4 &= K_{4,0}\,\Delta t \end{aligned}\right\} \tag{A3}$$

With $\Delta t = 0.05$ s the following was found to be a suitable setting: $K_{1,0} = 4$, $K_{2,0} = 4$, $K_{3,0} = 1$, $K_{4,0} = 20$, ω_m equal to typical frequency, p_a equal to typical amplitude.

Time to next crest or through

$$\varphi = \text{arctg}\left(\frac{\hat{p}_2}{\hat{p}_1\hat{\omega}}\right) \qquad , \varphi \in [0,\pi\rangle \tag{A4}$$

$$t_t = \frac{\varphi}{\omega} \tag{A5}$$

The buoy is to be released if t_t is less than the specified release time t_s.

New a priori estimates

$$\left.\begin{aligned} \bar{p}_1 &= \hat{p}_1 + \hat{p}_2\Delta t \\ \bar{p}_2 &= (1 - \hat{\omega}^2\Delta t^2)\,\hat{p}_2 - \hat{\omega}^2\hat{p}_1\Delta t \\ \bar{\omega} &= \hat{\omega} \\ \bar{p}_\ell &= \hat{p}_\ell \end{aligned}\right\} \tag{A6}$$

APPENDIX B. POWER ABSORPTION BY A HEAVING, SEMI-SUBMERGED, PHASE CONTROLLED BUOY IN REGULAR WAVES

The radiation resistance in heave for a semi-submerged sphere can be written as

$$R(\omega) = \rho V \omega \varepsilon(\omega) \tag{B1}$$

where V is the deplaced volume. Greenhow [8] has suggested the following analytical expression for the function ε

$$\varepsilon(\omega) = \frac{ka}{3.6(ka)^2 + 0.56} \tag{B2}$$

where k is the wave number and a is the radius of the sphere. Falnes [9] has proposed the following correction to eq. (B2)

$$\varepsilon(\omega) = \frac{ka}{3.6(ka)^2 + 0.56 - \delta_1(\omega) + \delta_2(\omega)} \tag{B3}$$

with

$$\delta_1(\omega) = 0.136 \exp\left\{-120(ka)^2/(1 + (ka)^2)\right\} \tag{B4}$$

$$\delta_2(\omega) = 0.074(ka)^5 \left\{1 + \frac{9(ka - 1.2)}{(ka)^3 + 1}\right\} \tag{B5}$$

The excitation force coefficient on deep water is given as

$$\kappa(\omega) = \sqrt{2\rho R(\omega) \frac{g^3}{\omega^3}} \tag{B6}$$

The buoy radiates waves at frequencies $n\omega_o$ where ω_o is the frequency of the incident wave and n is any odd number ($n = 1, 3, 5...$). The absorbed power can then be written as [10].

$$P_t = \tfrac{1}{2}\kappa(\omega_o)\eta_o C_1 s_m \omega_o \cos\varphi - \tfrac{1}{2}\sum_{n=1,3,5..} R(n\omega_o)\ (n\omega_o C_n s_m)^2 \qquad (B7)$$

where

$$C_n = \frac{4}{\pi}\ \frac{\cos(\frac{\pi}{2}\, n\gamma)}{1 - (n\gamma)^2} \qquad (B8)$$

$$\gamma = \frac{T_b}{T_o} \qquad (B9)$$

$$\varphi = 2\pi \cdot \left(\frac{t_\varphi}{T_o}\right) \qquad (B10)$$

As shown in fig. B1 the wave amplitude is η_o and s_m is the stroke amplitude of the buoy. The time difference between the wave and the buoy velocity is t_φ. The period of the incident wave is T_o and the natural period of the buoy is T_b.

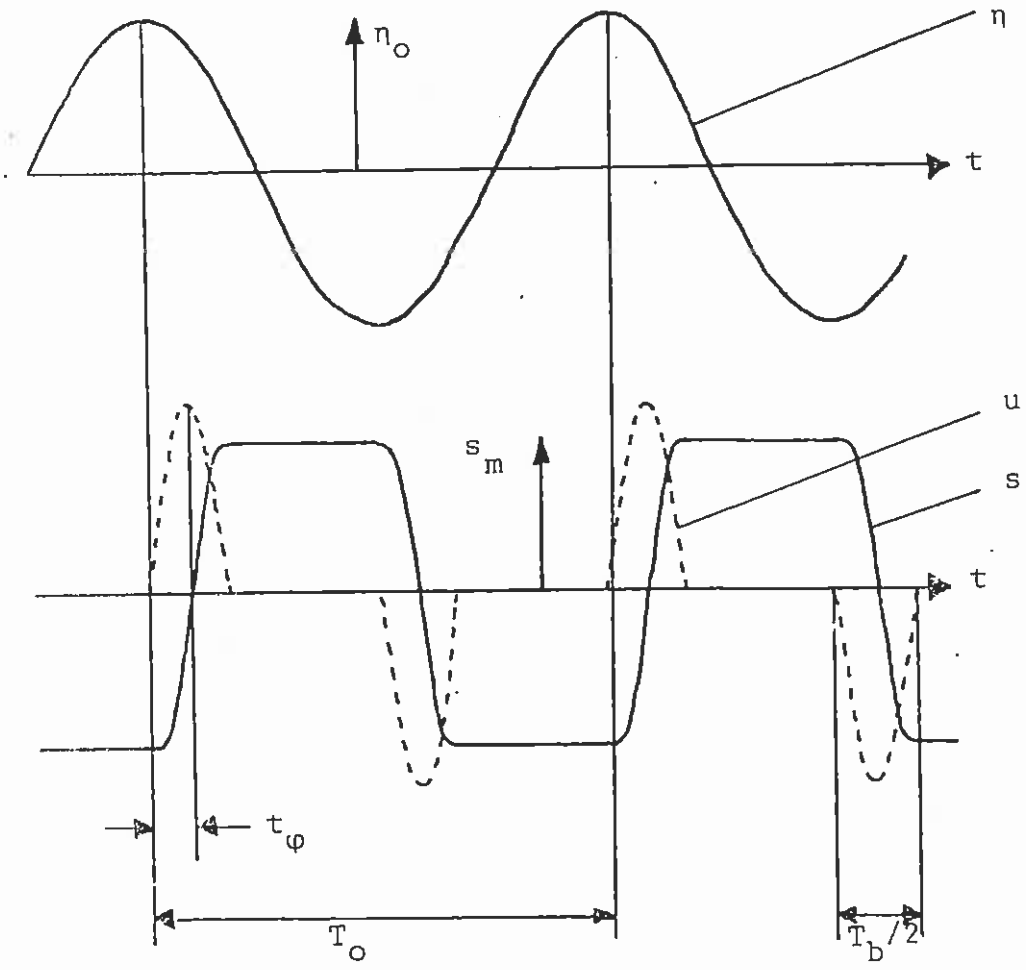

Fig. B1 Definition of T_o , η_o , T_b , s_m and t_φ.

η: The wave elevation.

s: The buoy position.

u: The buoy velocity.

REFERENCES

[1] K. Budal, J. Falnes, L.C. Iversen, P.M. Lillebekken, G. Oltedal, T. Hals, T. Onshus and A.S. Høy, The Norwegian wave-power buoy project, The Sec.Int.Symp. on Wave Energy Utilization, Trondheim, pp. 323-344 (1982).

[2] L.C. Iversen, T.I. Waag, Anskaffelse av VAX 11/750 til bølgekraftprosjektet, Inst. for eksp.fysikk, NTH, mars 1981.

[3] L.C. Iversen, PC - Programsystem for prosesskontroll med VAX-11 datamaskin i kombinasjon med LPA11-K., Inst. for eksp.fysikk, NTH, des. 1982.

[4] A. Høy, Kalibrering av måleblender, NSFI rapport O.R. 23.1142.00.01.82, 1982.

[5] T. Onshus, Optimal phase control of power-buoy, SINTEF report STF48 F79038 (1979).

[6] K. Budal, J. Falnes, L.C. Iversen, T. Hals and T. Onshus, Model experiment with a phase-controlled point absorber, Sec.Int.Symp. on Wave and Tidal Energy, Cambridge, pp. 191-206 (1981).

[7] G.F. Knott and J.O. Flower, Energy losses in oscillatory flow through a pipe exit, Applied Ocean Research, 2, pp. 155-164 (1980).

[8] J.L. Greenhow, Approximate models of a heaving sphere with linear and non-linear power take-off mechanism, Inst. for marin hydrodyn., NTH, feb. 1981.

[9] J. Falnes, Empirisk formel for Havelock $\varepsilon(ka)$, Inst. for eksp.fysikk, NTH, feb. 1982.

[10] L.C. Iversen, Power conversion from regular waves by heaving buoy with limited amplitude, Internal Report, Inst. for eksp.fysikk, NTH, Revised version feb. 1982.